nuclear fusion
IAEA

ACCEPTED MANUSCRIPT • OPEN ACCESS

Inter-machine plasma perturbation studies in EU-DEMO relevant scenarios: lessons learnt for EM forces prediction during VDEs

To cite this article before publication: Giuliana Sias *et al* 2022 *Nucl. Fusion* in press https://doi.org/10.1088/1741-4326/ac544b

Manuscript version: Accepted Manuscript

Accepted Manuscript is "the version of the article accepted for publication including all changes made as a result of the peer review process, and which may also include the addition to the article by IOP Publishing of a header, an article ID, a cover sheet and/or an 'Accepted Manuscript' watermark, but excluding any other editing, typesetting or other changes made by IOP Publishing and/or its licensors"

This Accepted Manuscript is **© 2022 The Author(s). Published by IOP Publishing Ltd.**.

As the Version of Record of this article is going to be / has been published on a gold open access basis under a CC BY 3.0 licence, this Accepted Manuscript is available for reuse under a CC BY 3.0 licence immediately.

Everyone is permitted to use all or part of the original content in this article, provided that they adhere to all the terms of the licence https://creativecommons.org/licences/by/3.0

Although reasonable endeavours have been taken to obtain all necessary permissions from third parties to include their copyrighted content within this article, their full citation and copyright line may not be present in this Accepted Manuscript version. Before using any content from this article, please refer to the Version of Record on IOPscience once published for full citation and copyright details, as permissions may be required. All third party content is fully copyright protected and is not published on a gold open access basis under a CC BY licence, unless that is specifically stated in the figure caption in the Version of Record.

View the article online for updates and enhancements.

This content was downloaded from IP address 93.144.194.240 on 28/03/2022 at 13:23

Inter-machine plasma perturbation studies in EU-DEMO relevant scenarios: lessons learnt for EM forces prediction during VDEs

G. Sias[1], S. Minucci[2], M. Lacquaniti[1], R. Lombroni[2], A. Fanni[1], G. Calabrò[2], B. Cannas[1], F. Pisano[1], M. Siccinio[3,4] G. Ramogida[5], F. Giorgetti[5], P. Fanelli[2], F. Maviglia[4,5], the EUROfusion MST1 Team* and JET EFDA Contributors**

[1] *Electrical and Electronic Engineering Dept.-University of Cagliari, Piazza D'Armi, 09123, Cagliari, Italy.*

[2] *Department of Economy, Engineering, Society and Business (DEIm), University of Tuscia, Largo dell'Università snc, Loc. Riello, 01100 Viterbo, Italy*

[3] *Max-Planck-Institut für Plasmaphysik, Garching bei München, Germany*

[4] *EUROfusion – Programme Management Unit, Boltzmannstrasse 2, 85748 Garching, Germany*

[5] *Associazione EURATOM-ENEA sulla Fusione, C.R. Frascati, C.P. 65-00044 Frascati, Rome, Italy*

** See Labit et al 2019 (https://doi.org/10.1088/1741-4326/ab2211) for the EUROfusion MST1 team.*

** See the author list of Overview of JET results for optimising ITER operation by J. Mailloux et al. to be published in Nuclear Fusion Special issue: Overview and Summary Papers from the 28th Fusion Energy Conference (Nice, France, 10-15 May 2021)

Corresponding author: simone.minucci@unitus.it

Abstract

To support the deployment of DEMO wall protection strategy, the development of comprehensive analyses is essential to understand the implications of transient perturbations on the plasma shape control and on the vertical stability, some of the most critical aspects to be considered in elongated plasmas. Therefore, the design activities of the DEMO limiter structures need the deep understanding of the effects induced by transient plasma perturbations coupled with one of the most severe load conditions occurring in tokamaks, the Vertical Displacement Event (VDE). Since Electromagnetic (EM) loads during VDE phases are among the DEMO limiters design drivers, this study focuses on predictive simulations of the final plasma position and of EM loads following a VDE. For this purpose, a multi-tokamaks study supported by the construction of an inter-machine database containing experimental transient plasma perturbations and VDEs from JET and ASDEX Upgrade (AUG) has been carried out. It aims at the characterization of some transient plasma perturbations that may lead to high control efforts by the vertical stability system in terms of variations of the plasma internal parameters and vertical displacements. Consequently, such experimental transient plasma perturbations have been properly scaled to DEMO reference geometries with different magnetic configurations, to be simulated in terms of plasma dynamical behaviour by means of MAXFEA code. Finally, initial predictive EM loads on DEMO limiter structures will be discussed in the case of VDEs following plasma perturbations.

Keywords: DEMO; Inter-machine database; Plasma perturbations; VDE; MAXFEA; Electromagnetic Analysis

1. Introduction

The plasma vertical stability is one of the most challenging aspects in the design of the demonstration fusion power plant, DEMO. This is mainly due to the presence of a thick Breeding Blanket (BB) system [1,2] placed between the plasma and the Poloidal Field (PF) coils, used as actuators for active plasma vertical stabilization purposes. The large PF Coils-plasma distance also implies a less effective passive stabilization effect of the Vacuum Vessel (VV) [3], resulting in an increase of the power needed to control the plasma vertical position,

Accepted Manuscript

especially in the case of off-normal operations inducing significant variations of the plasma internal parameters. Moreover, even if the present DEMO BB concept design can withstand heat loads compatible with the foreseen steady state and controllable transient conditions [4], greater challenges arise from the occurrence of severe off-normal events like VDEs [5, 6]. Hence, it is essential to develop comprehensive analyses to understand the implications of transients and off-normal events on the plasma vertical stability.

In the present fusion devices, several transient plasma perturbations have been experienced during the experimental campaigns, as Edge Localized Modes (ELMs) [7], transitions from high to low confinement modes and vice versa (H-L/L-H transitions) [8], and minor disruptions (mDs) [9]. The occurrence of such perturbations is strongly connected to variations of plasma internal parameters and, consequently, to a plasma displacement [10], which may lead to high control efforts by the vertical stability (VS) system.

If they are coupled with the natural vertical instability of the plasma, transient plasma perturbations could trigger, ultimately, a VDE with the plasma colliding with the upper or lower part of the internal plasma facing components (PFCs), with subsequent electrical currents able to flow into the VV. These currents cross the magnetic field of the tokamak, generating large EM loads that are often the design drivers of tokamak First Wall (FW) and of other components. Hence, 2D/3D electromagnetic simulations [11,12,13,14] aimed at understanding the implication of these transients on the plasma vertical stability are essential. Since a strategy based on the use of discrete high heat flux limiters is being proposed and developed for DEMO FW, it is necessary to identify locations of plasma-wall contact during VDEs to design a limiter configuration capable to protect the breeding wall under all circumstances. In [15], it has been shown that it is possible to predict the plasma-wall contact point in case of VDE by evaluating the plasma magnetic flux map before the disruption and by setting the disruption duration.

In this paper, an innovative approach is proposed as methodology to deal with the criticality of vertical stability as a driver in the design of the DEMO limiter structures: first, an inter-machine experimental database of transient plasma perturbations in standard Single Null (SN) and in Quasi Double Null (QDN) configurations has been built with JET and ASDEX Upgrade (AUG) experiments. Among plasma transients, the variation of the plasma centroid vertical position is correlated to that of the plasma internal parameters (i.e., poloidal beta β_{pol} and internal inductance l_i) and their time derivatives during Edge Localized Modes (ELMs), Low-to-High Confinement (L-H) and H-L transitions. Consequently, such experimental transient plasma perturbations have been properly scaled to DEMO reference geometries [16, 17] with different magnetic configurations, to be simulated in terms of plasma dynamical behaviour by means of MAXFEA code [18]. Finally, initial predictive EM loads on DEMO limiter structures are discussed in the case of VDEs coupled with H-L transitions and Major Disruptions (MDs) perturbations.

The aforementioned methodology procedure that will be described in detail later in the paper is summarized by means of the flowchart shown in Figure 1 as consequent steps:

1. JET-AUG inter-machine database has been built to characterize the plasma vertical displacement w.r.t. the plasma internal parameters variation in case of occurrence of transient plasma perturbations;
2. equilibrium reconstructions, simulation of the plasma perturbation and validation of the reconstructed dynamics w.r.t. the experimental ones in JET and AUG devices have been set up by means of MAXFEA plasma evolution code;
3. experimental VDEs following plasma perturbations have been simulated by MAXFEA code;
4. experimental inter-machine plasma perturbations have been properly scaled to DEMO and simulated by MAXFEA code;
5. finally, VDE following plasma perturbations have been simulated using MAXFEA code and discussed in terms of EM loads on DEMO limiter structures.

Accepted Manuscript

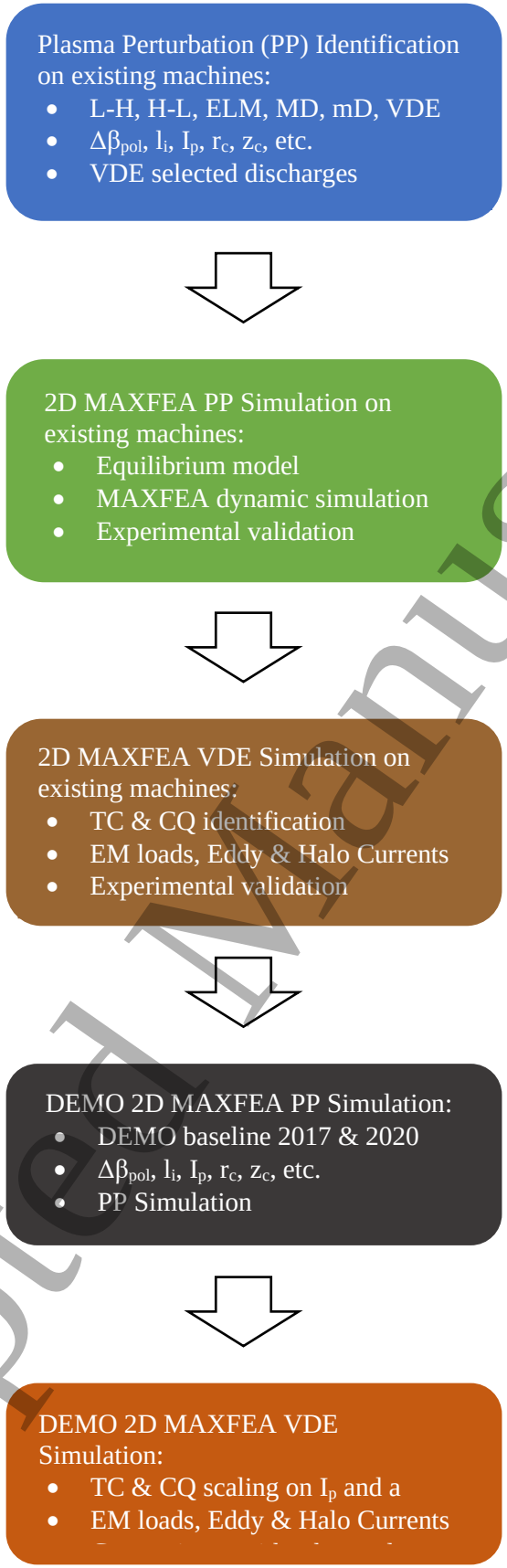

Figure 1: Flowchart of the procedure used to perform predictive EM analyses on scaled-to-DEMO configurations in the case of plasma perturbations coupled to vertical displacement events

Accepted Manuscript

The structure of the paper follows the procedure shown in Figure 1. Section 2 reports the description of the plasma perturbations and off normal events inducing variations in the plasma shape and position, and the algorithms and criteria used to select the perturbations of interest. Section 3 details the structure of the inter-machine database. It should be noted that the information reported into the database have been tailored on the needs of the studies developed in this work. Section 4 is dedicated to the characterization of the vertical displacement during ELMs, L-H and H-L transitions, featured by the variation of β_{pol} and l_i and their time derivatives, for JET experimental data. Section 5 reports the results of the MAXFEA reconstruction of the plasma dynamic behaviour, suitably scaled to DEMO, starting from experimental data. Experimental plasma transients are used as guideline in the investigation of the plasma vertical displacement and of the evaluation of EM loads on Vacuum Vessel (VV) during a set of possible VDEs. Among plasma transients, H-L transitions and mDs have been considered, the latter both in SN and QDN configurations. The extrapolation to DEMO has been realized using the most recent DEMO reference geometries (2017 and 2020) [19]. Finally, the main conclusions are given in Section 6.

2. Plasma perturbations

Experiments affected by transient plasma perturbations (ELMs, L-H/H-L transitions and mD) and VDEs have been selected from JET and AUG experiments in standard SN and in QDN configurations, with the purpose of characterize the plasma perturbation in terms of variation of its vertical position and internal parameters. Algorithms and criteria developed for selecting the discharges affected by the considered perturbations are illustrated in the following sections.

2.1 Vertical Displacements

In elongated plasmas, the vertical position must be feedback controlled since the loss of control causes hot VDEs. Even when the disruption itself is not induced by a vertical instability, it is common that the final loss of plasma current is associated to a VDE. Large vertical displacements are characterized by a sudden and large change of plasma parameters which, among others, affects the vertical feedback control.
According to ITER Physics [20], plasma disruptions are usually classified depending on the position of the plasma column at the thermal quench (TQ), as MDs and VDEs.

- Major Disruption, when the thermal quench occurs with the plasma close to its neutral position (Central Disruptions) and a loss of position control is often experienced after the thermal quench (cold VDE).
- In Up and Down VDE (UVDE and DVDE), a loss of position control destabilizes the plasma before the TQ, occurring when the plasma touches the wall or at a given critical safety factor.

In this work, disruptions have been labelled from the perspective of the vertical displacement event occurrence and taking into account the Massive Gas Injection (MGI) system action, as follows:

- Type 1 VDE is the so-called hot VDE: a large plasma vertical displacement (several centimetres) induces a MD and the MGI (if any) follows the MD, as in the example reported in Figure 2 for an AUG pulse. The blue line reports the plasma current; the dashed red line indicates the time when the final collapse occurs, assumed as disruption time t_D, and the brown line reports the actual plasma vertical position Z_c. In this case no action is taken by the MGI system.
- Type 2 VDE: a large plasma vertical displacement activates the MGI that, in turn, induces a disruption. In Figure 3, an example of a disruption induced by the killer gas injection at AUG is shown. The potential consequences of a downwards movement of the plasma column are prevented by the MGI. The dashed green line in Figure 3 indicates the killer gas puffing onset (t_{kG}); in 3 *ms*, this results in a disruption (black dashed line).
- Type 3 VDE is the so-called cold VDE: a large vertical displacement follows a MD and the MGI (if any) is triggered in the late Current Quench (CQ). In Figure 4, a Type 3 VDE at JET is shown: the

Accepted Manuscript

killer gas puffing onset (green dashed line) follows the large vertical displacement due to the disruption (black dashed line).

Another type of VDE (Type 4) can be defined when the MGI follows the disruption and precedes the VDE, but it is not interesting for the present study because the VDE is affected by the MGI. Referring to the ITER Physics classification [20], Type 1 and Type 2 fall into VDE category, whilst Type 3 and Type 4 fall into MD category. Note that, no distinction has been made between upward and downward displacement in this paper.

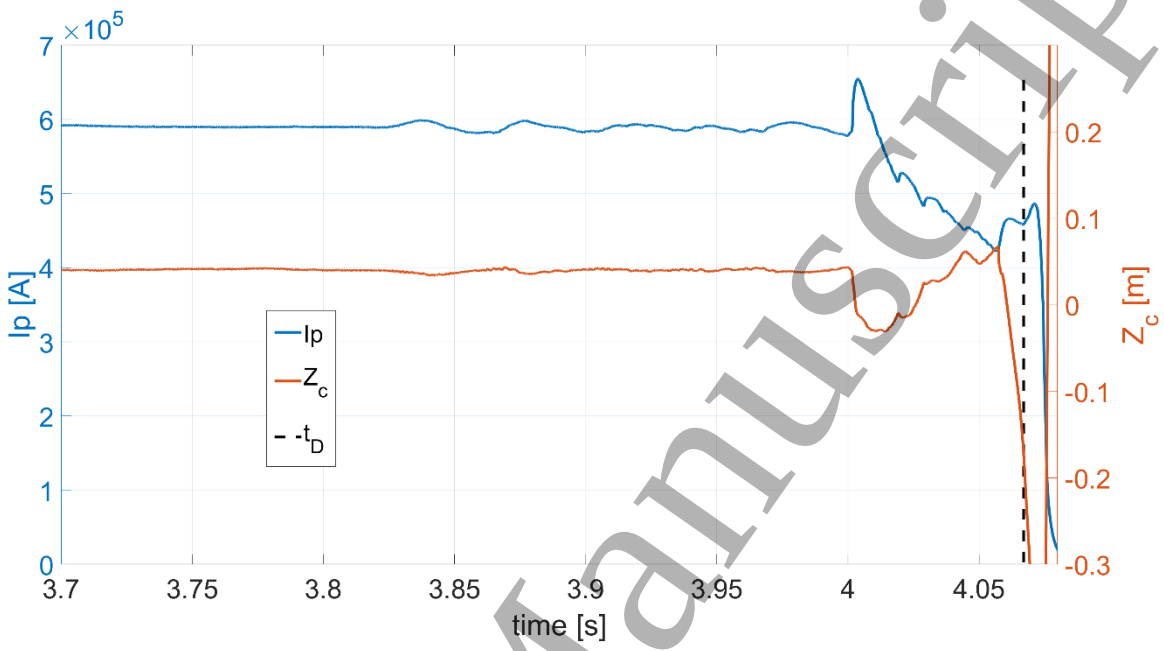

Figure 2. AUG pulse #29462, Type 1 VDE. A deviation larger than 15 *cm* of Z_c (brown line) is reached at the disruption time highlighted with a red dashed line on the plasma current (I_p) evolution (blue line). In Type 1 VDE, a large vertical displacement induces the disruption. No action is taken by MGI.

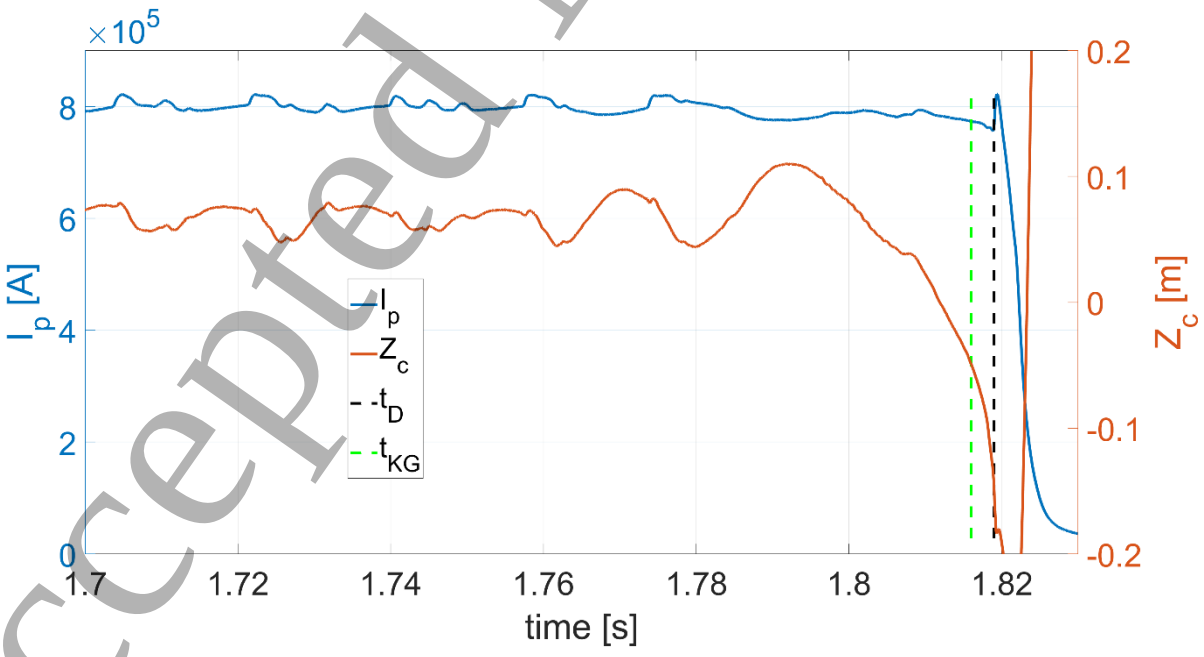

Figure 3. AUG pulse #29515, Type 2 VDE. A deviation of Z_c (brown line) of about 10 *cm* activates the MGI system (green dashed line), in turn inducing the disruption highlighted with a black dashed line on the plasma current (I_p) evolution (blue line). In a Type 2 VDE, the MGI interrupts a larger vertical displacement.

Accepted Manuscript

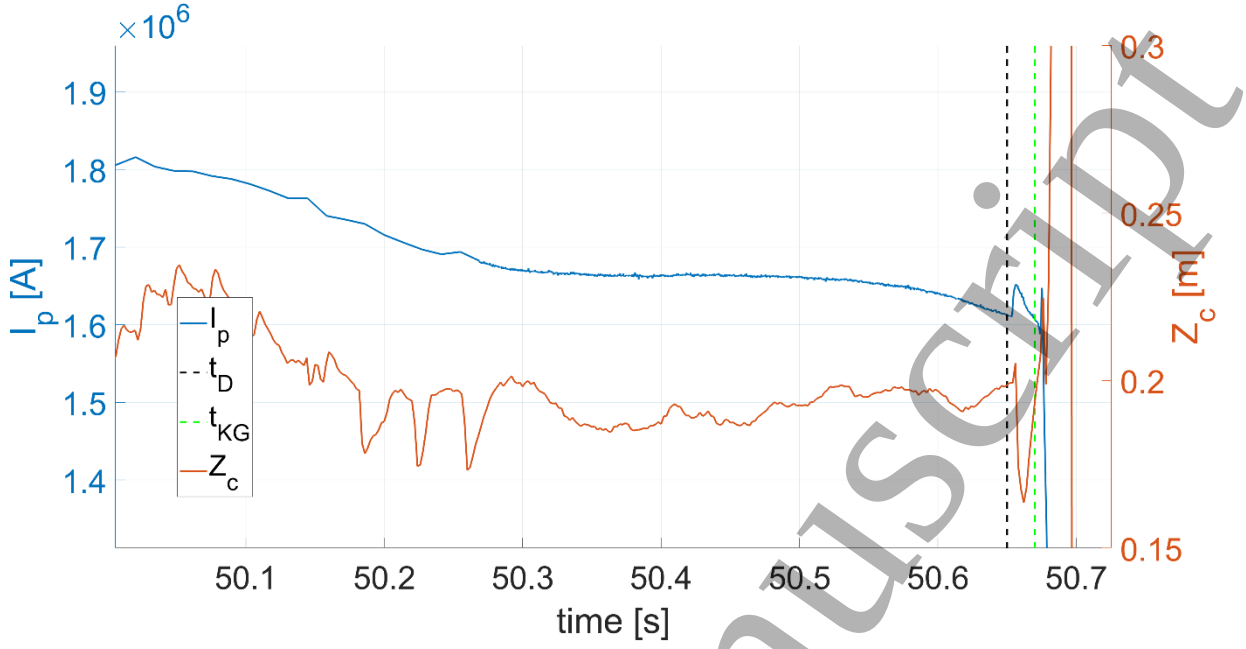

Figure 4. JET pulse #92100, Type 3 VDE. A large deviation in Z_c (brown line) is observed after the disruption time (black dashed line) during the CQ phase (blue line). The MGI is activated during the CQ. In a Type 3 VDE, a large vertical displacement is induced by a MD.

In [21], the automatic detection of VDEs at AUG was obtained by evaluating the deviation of the actual vertical position Z_c with respect to the reference vertical plasma position signal (Z_{ref}). At JET, an algorithm based on the evaluation of the normalized vertical position is proposed in [22]. In this paper, a simple approach is proposed to perform both the automatic detection and the classification of VDEs, following the types defined above, for both the considered machines.

The algorithm evaluates the absolute deviation of Z_c (Z_{c_DEV}) from its own mean value in the last time window *tW*, at each time. The *tW* length and the threshold value discriminate if the VDE occurs before (Types 1 and 2) or after (Type 3) the disruption time and have been optimized for JET and AUG on VDE databases previously manually classified. Finally, the discrimination between Type 1 and Type 2 is performed considering the temporal consecution of t_{kG} and t_D. Note that, the proposed algorithm can be used even when the Z_{ref} signal is not available or if an offset is present.

2.2 Minor disruptions

During a minor disruption event, a temporary degradation of the plasma energy confinement occurs, the stored energy (W_{mhd}) is not completely released and an ohmic heating recovering of the discharge is observed [11]. Figure 5 shows a minor disruption occurring at the plasma current flat-top for a JET pulse; it takes place at 50.8 s ($t_{start\text{-}mD}$, dashed green vertical line), the energy is recovered at 51.55 s ($t_{end\text{-}mD}$, dot green vertical line), and a MD occurs about 1 s later.

Accepted Manuscript

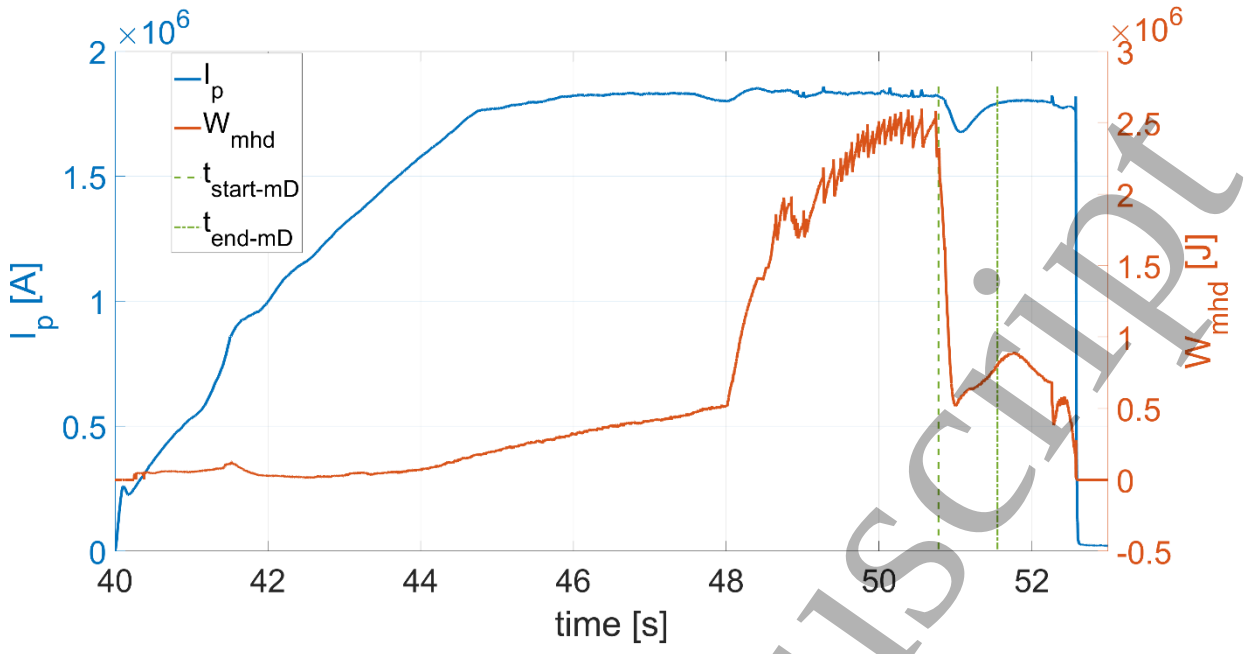

Figure 5. JET pulse #89604: flat-top minor disruption. W_{mhd} in brown, I_p in blue, mD starting ($t_{start\text{-}mD}$) and ending ($t_{end\text{-}mD}$) times are indicated by the dashed and dot green vertical lines.

An algorithm for the automatic detection of the starting ($t_{start\text{-}mD}$) and the ending ($t_{end\text{-}mD}$) times of mDs, occurred during the plasma current flat-top, has been developed. As for the MDs, the starting of the event results in a plasma current spike corresponding to a sudden variation of the internal inductance (l_i) and a drop of the plasma energy W_{mhd}. The evolution of the mD is characterized by a plasma current groove followed by a complete recovery that occurs when the release of W_{mhd} stops, and the plasma current is resumed.
The mD automatic detection is performed by computing the absolute deviation of I_p, l_i and W_{mhd} signals at each time with respect to their own mean values in a previous time window tW. A minimum and a maximum threshold have been optimized for the deviation of each signal. The time when the three differences exceed their own maximum threshold is assumed as the minor disruption starting time. The energy confinement is totally recovered when the three deviations fall below the minimum values of their own thresholds.

2.3 L-H/H-L transitions and ELMs

A good confinement is critical to plasma reactor performance. The preferred route to good confinement is the high confinement mode (H-mode), characterized by the spontaneous build-up of steep density and pressure gradients at the plasma edge. The Edge Localized Modes (ELMs) are MHD instabilities, occurring at the edge of H-mode plasmas, which appear as repetitive events leading to a fast (≈ms) loss of energy and particles from the plasma edge [23].
In this work, both L-H/H-L transitions have been classified as slow or fast according to the methodology reported in [24-25] and have been selected from dedicated experiments detailed in [26]. Figure 6 shows an example of slow L H/H L transitions for a JET pulse. The figure reports, from top to bottom, the NBI power (P_{NBI}), the photon flux near the divertor target plates (D_α), the average electron density (n_e), and the diamagnetic energy (W_{DIA}) repelled by the plasma. It should be noted that for both slow and fast aforementioned plasma perturbations, average electron density is reported only for the pronounced increase (i.e., plasma perturbation L-H phase) and consequently full increase (i.e., constant additional heating) in the middle of flat-top phase. The slow L-H transition is experimentally obtained by a slow increase of the additional power injected into the plasma, and it is characterized by a pronounced increase of n_e and W_{DIA}, followed by an increase of D_α [24].

Accepted Manuscript

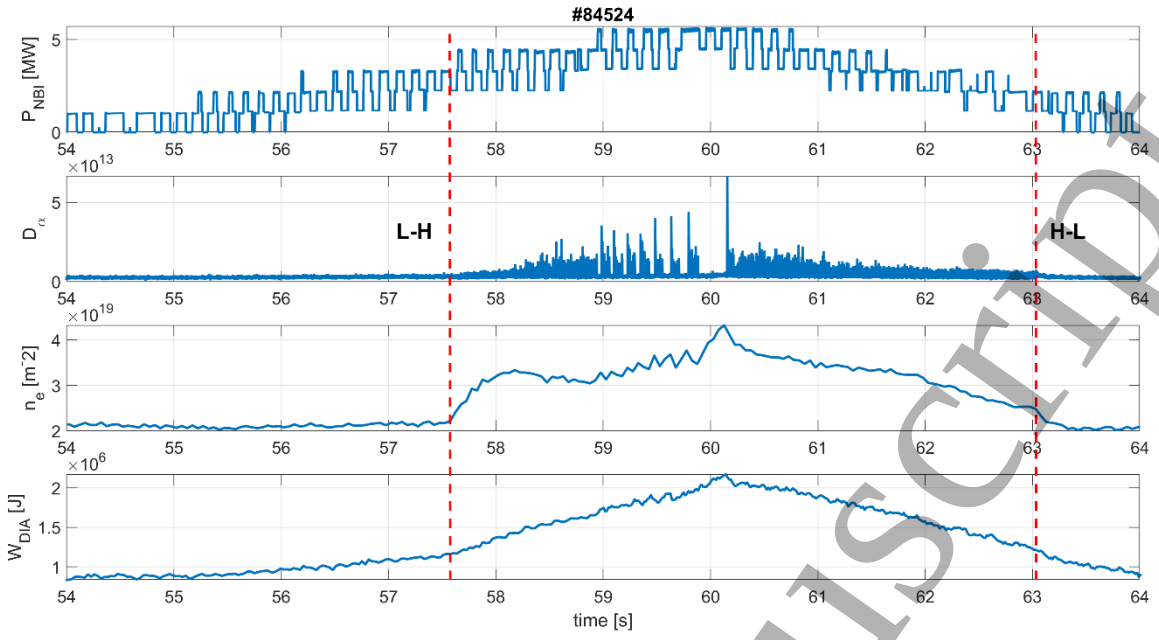

Figure 6. JET pulse # 84524: slow L-H and H-L transitions. Total heating power (top row), D_α (second row) in a.u., average electron density (third row) and diamagnetic energy repelled by the plasma (bottom row). The vertical dashed red lines indicate the slow L-H and H-L transitions.

On the other hand, a fast L-H transition is obtained by a fast increase of the additional power injected into the plasma and is characterized by a sharp increase of n_e and W_{DIA} and an increase of D_α [24]. What above is shown in Figure 7 in correspondence of the first vertical red dashed line. On the contrary, a fast H-L transition follows a decrease of the additional power injected into the plasma and is characterized by a sharp decrease of n_e and W_{DIA} and a decrease of D_α [24] (see the second vertical red dashed line). The methodology used for L-H/H-L identification is explained in Section 3.3, following similar approach discussed in [25].

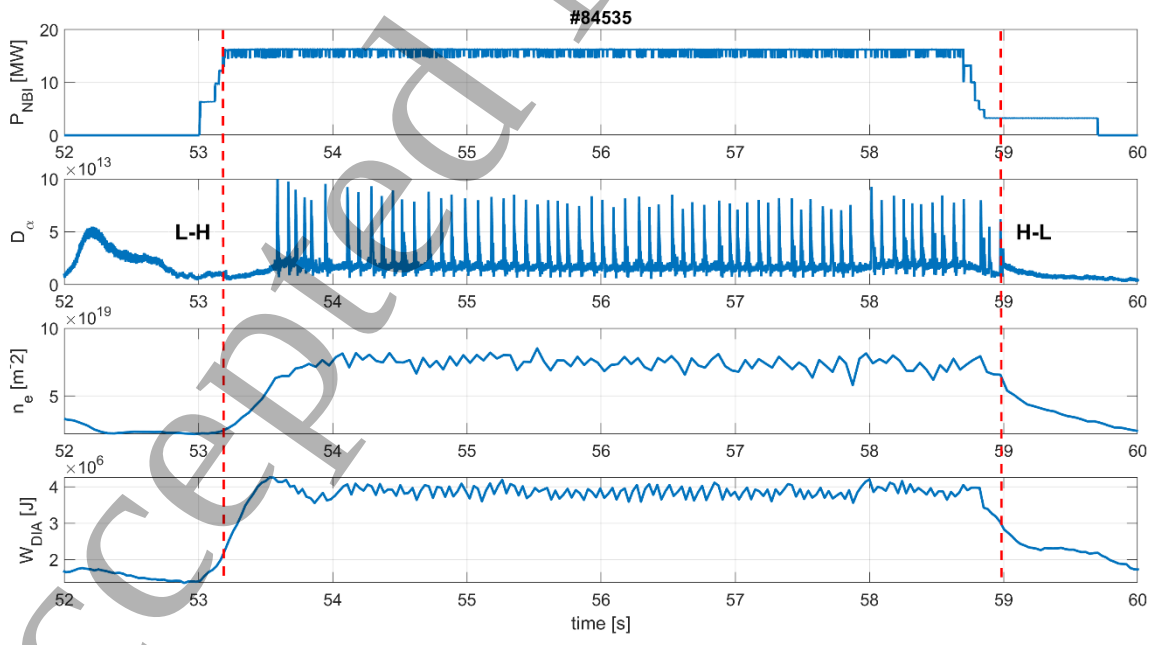

Figure 7. JET pulse #84835: fast L-H and H-L transitions. Additional Power (top diagram), D_α (second top diagram) in a.u., average electron density (third top diagram), diamagnetic energy repelled by the plasma (bottom diagram) in a significant time window. ELMs have been observed during the H-mode phase. The vertical dashed red lines indicate the fast L-H and H-L transitions.

Accepted Manuscript

The ELM perturbation database has been populated with what reported in the reference experiments [26]. Typically, the effect of the L-H/H-L transitions and ELMs on β_{pol} and Z_c parameters for the selected JET discharges can be summarized as follows:

- SLOW L-H/H-L: small variation of the poloidal beta ($\Delta\beta_{pol}\% \approx 5\%$) that leads to a small variation of the vertical position of the plasma centroid ($\Delta Z_c \approx 1mm$).
- FAST L-H/H-L: high variation of the poloidal beta ($\Delta\beta_{pol}\% \approx 50\%$) that leads to a small variation of the vertical position of the plasma centroid ($\Delta Z_c \approx 6mm$).
- ELM: moderate variation of the poloidal beta ($\Delta\beta_{pol}\% \approx 20\%$) that leads to a high variation of the vertical position of the plasma centroid ($\Delta Z_c \approx 40mm$).

3. Inter-machine database of plasma perturbations

Several algorithms have been developed to support the construction of the intermachine database; besides those discussed in Section 2, other algorithms are presented in this section which provide information about characteristic times and phases (flat-top, thermal quench and current quench), the killer gas puffing onset, the H-L transition time, and the plasma configuration. Moreover, the database collects information about the additional heating powers and the values of the main plasma parameters in prefixed time windows.

3.1 Characteristic times

When constructing a database collecting plasma perturbations during the plasma current flat-top phase, the first step is the flat-top identification according to the pulse termination behaviour, disrupted or regular. For a regular terminated pulse, plasma current flat top is defined by two time instants: the starting time t_0, corresponding to the end of the ramp up phase, and the ending time t_f, corresponding to the start of the ramp down phase. On the other hand, for a disrupted discharge, the flat top ending time is the disruption time t_D, which has been assumed within the thermal quench phase. In particular, the time selected corresponds to the drop of the core temperature and the start of the plasma current spike due to the sudden variation of the internal inductance. An algorithm for the automatic flat top identification has been developed. As a first step, a threshold on the time derivative value of the pre-programmed current has been optimized to select t_0, which defines the minimum slope for the ramp-up phase. Once t_0 is detected, for each time after t_0, the algorithm selects all current spikes with a slope larger than an optimized threshold and having an absolute value of l_i time derivative larger than a certain threshold in the time window of the current rising phase. Finally, the time corresponding to the largest percentage variation of l_i and I_p during the current spike frame is selected as the disruption time t_D. Since some VDEs are characterized by a sudden CQ not preceded by a plasma current spike, if no t_D is detected so far, a check is performed on the CQ rate. If the CQ slope is lower than an optimized threshold, the discharge is assumed to be a VDE, and the last point of the flat top is assigned as t_D. Otherwise, the discharge is regularly terminated, and the final point of the flat top is labelled as t_f. After detecting the flat-top phase, the starting and the ending time of CQ ($t_{start\text{-}CQ}$, $t_{end\text{-}CQ}$) are selected based on both the value of the I_p time derivative and the I_p fraction value, which is evaluated with respect to the I_p flat-top value.

To optimize the different thresholds used in the algorithm, the characteristic times in a set of discharges in the database have been manually identified, and the corresponding thresholds have been selected by minimizing the errors made using the automatic identification of the aforementioned times.

3.2 Massive Gas Injection time

At JET and AUG, the killer gas puffing is performed by means of three valves. In this work, the time when the killer gas is injected into the vessel (t_{kG}) is automatically detected for the three valves: t_{kG} is assumed as the time when a sudden change in the killer gas pressure occurs, shortly after the MGI trigger onset for AUG, and after the MGI power system shutdown for JET.

3.3 L-H/H-L transition times and ELM time window

Accepted Manuscript

In this work a database of ELMs and L-H/H-L transitions has been built, from dedicated experiments detailed in [26], to feature the effect of the transients in terms of relation between the plasma vertical displacement and the variation of the plasma internal parameters β_{pol}, and l_i (see Section 4) and their time derivatives.
The identification of endpoints of the H-mode time window (i.e., the L-H transition start and the H-L transition end) for both slow and fast transitions has been performed by manually analysing the time traces of the parameters shown in Figure 6 and Figure 7, respectively. The time instants are identified as those when a change in the slope of n_e and W_{DIA} (positive for L-H and negative for H-L transitions) occurs, together with a drop or a step up into D_α signal, for the L-H and the H-L transitions respectively.
For each ELM, a time window ($t_{start\text{-}ELM} \div t_{end\text{-}ELM}$) has been defined by detecting the maximum and minimum values in the oscillation of β_{pol}, Z_c, and D_α time traces, as highlighted in Figure 8, where the red and green lines indicate the stating and the ending times, respectively. The time window ($t_{start\text{-}ELM} \div t_{end\text{-}ELM}$) is set according to the ELMs frequency (around 20 ms).

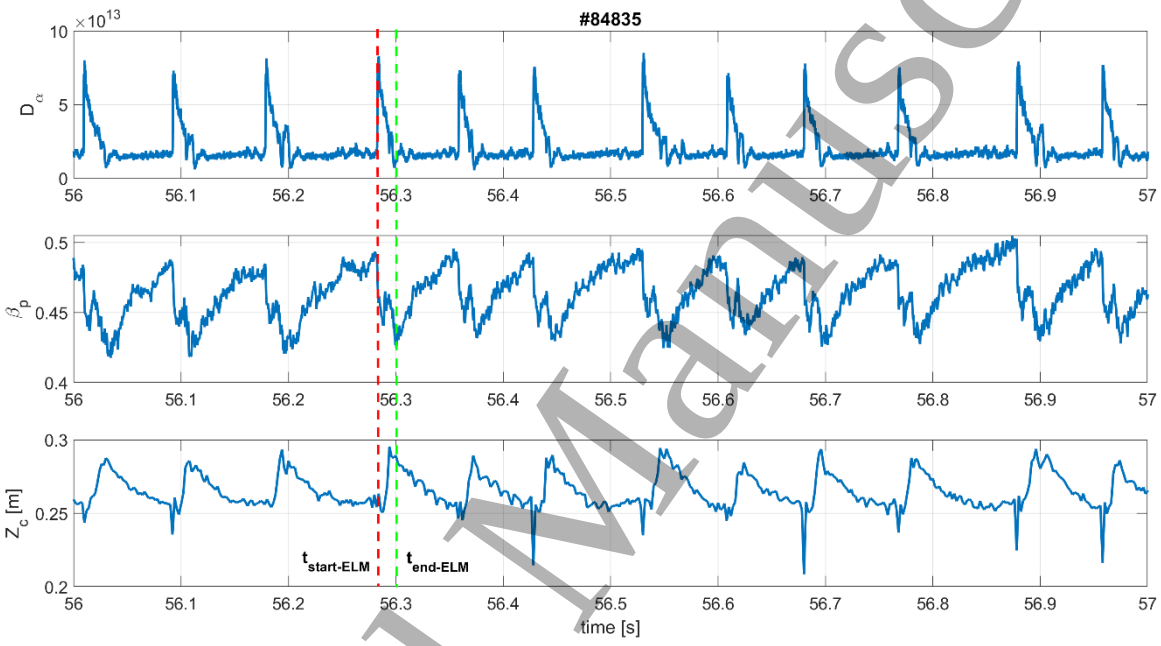

Figure 8. JET pulse # 84835: ELMs effect on D_α, β_{pol}, and Z_c time traces in a time window of 1s. The red and green lines indicate the starting ($t_{start\text{-}ELM}$) and the ending ($t_{end\text{-}ELM}$) times respectively, as selected for populating the ELM database.

Moreover, the last H-L transition (if any) has been detected for VDEs and mDs selected for this work. In fact, numerical simulations have been performed to evaluate the dynamic evolution of the plasma centroid for a VDE preceded by H-L transition, starting from the knowledge of the plasma internal parameters variations. The transition time has been detected following the criterion described above and adopted for the L-H/H-L transition database.

3.4 Plasma configuration

The exploration of DN configurations in DEMO seems to be promising [12], because of the decoupling of the vertical unstable mode from the plasma perturbations in case of ideal DN, with up-down symmetric passive structures. For this reason, it is interesting to evaluate this coupling in realistic conditions in present day machines, where a certain up-down asymmetry of their passive structures is present [12, 27]. As DN configurations are not available for JET and AUG experiments, a selection of minor disruptions and vertical displacement events occurred in QDN plasma configurations has been carried out. To this end, labelling if the plasma is in SN, or QDN configuration is another key information to be collected in the intermachine database. As the information about the QDN configuration during the phase of interest was not available at JET, an

Accepted Manuscript

algorithm has been developed based on the projection of the X-points on the poloidal plane. The tracking of the time variation of the upper ($Z_{xp,u}$) and lower ($Z_{xp,l}$) X-point positions with respect to the wall boundary easily allow the detection of the time instant when the upper X-point leaves the vessel. The monitoring of the plasma configuration and the automatic detection of the time instant when the QDN configuration is achieved or lost can be easily performed by means of the control of this information together with the minimum value reached by the triangularities (upper and lower, δ_u and δ_l respectively) and by the elongation (k). The reference values needed for elongation and triangularities to achieve the QDN are reported in [28] for both JET and AUG. Figure 9 tracks the lower and upper X-point positions (X_{pl} and X_{pu} respectively), by a shade from blue to yellow, on the JET C-Wall boundary for pulse #68808, during a mD occurring between 46.74s and 47.04s. Figure 10 shows the behavior of δ_u and δ_l (magenta and red lines respectively), k (green line), $Z_{xp,u}$ and $Z_{xp,l}$ (solid and dashed black lines respectively), $t_{start\text{-}mD}$ and $t_{end\text{-}mD}$ (cyan and blue vertical line, respectively). From 45.35s (QDN achieved) until $t_{start\text{-}mD}$, the triangularities and the elongation roughly fit the values indicated in [28]. During the minor disruption, elongation and triangularity values start to deviate from the reference values. At 46.83 s, $Z_{xp,u}$ starts to increase while the upper X-point (Xpu) approaches the first wall. The QDN configuration is definitely lost at 47.02 s when $Z_{xp,u}$ falls down and the upper X-point trajectory goes outside the first wall boundary.

Instead, the information about the QDN configuration drawn from the elongation and triangularities is not supported by projection of the X-points on the poloidal plane for AUG, but it is corroborated by the maximum variation of the distance between the two separatrices, defined by means of the proximity to DN configuration factor which must be lower than 10 mm [28].

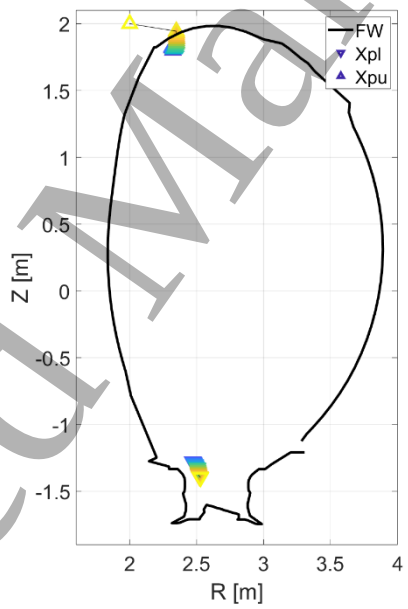

Figure 9. JET-CW pulse #68808: tracking of both the lower and upper X-point positions with respect to the JET-CW boundary on R-Z plane. The shade from blue to yellow tracks the upper and lower X-point positions during the minor disruption. The QDN configuration is lost at 47.02s when the upper X-point trajectory overcomes the first wall boundary.

Accepted Manuscript

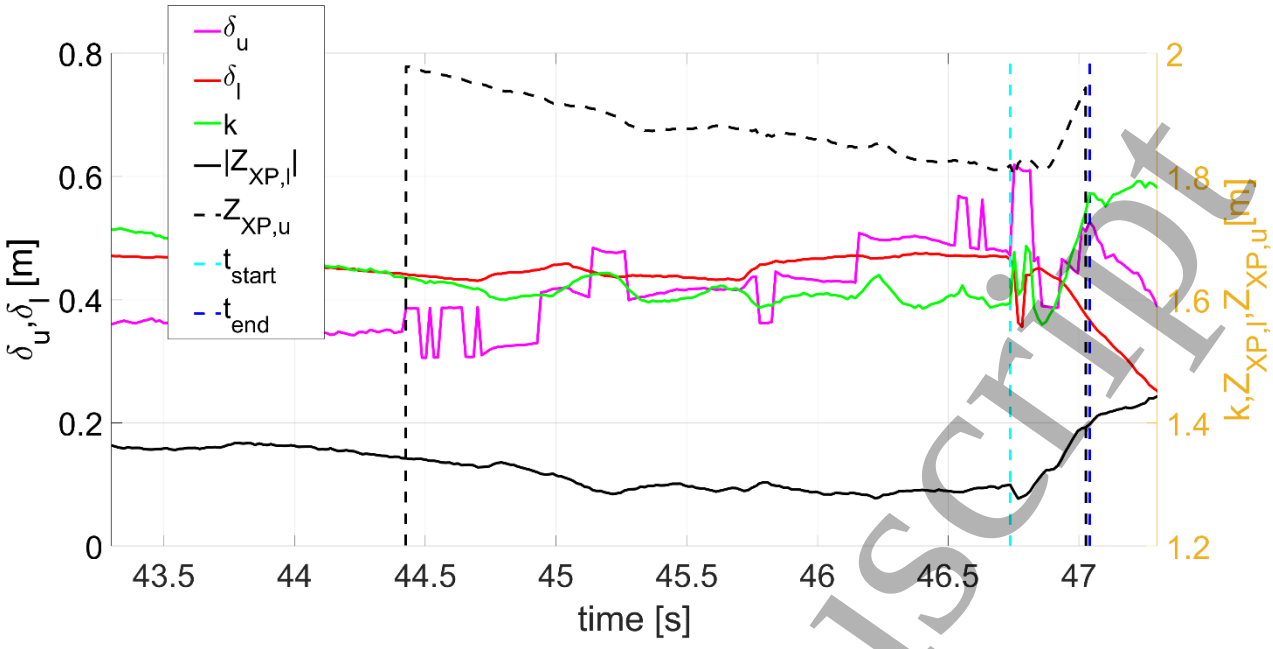

Figure 10. JET-CW pulse #68808: the behavior of triangularities (magenta and red lines for δ_u and δ_l respectively), elongation k (green line), $Z_{xp,u}$ and $Z_{xp,l}$ (solid and dashed black lines respectively), $t_{start\text{-}mD}$ and $t_{end\text{-}mD}$ (cyan and blue vertical line respectively) during the flat top phase. The QDN configuration is lost at 47.02s when $Z_{xp,u}$ falls down, δ_u, δ_l, and k deviate from the reference values and the upper X-point trajectory overcomes the first wall boundary.

3.5 Database structure

Hundreds of discharges have been analysed from JET ITER-like wall (JET-ILW) and AUG full tungsten wall. Moreover, since QDN is avoided in JET-ILW experiments due to the fragile ILW metal wall especially at high power level, a number of JET Carbon wall (JET-CW) experiments performed in 2006 [29] have been also analyzed for the selection of perturbations in QDN configuration.

Table 1 summarizes the characteristic times provided in the databases. For each pulse affected by the considered perturbation, information to identify the flat top phase (t_0, t_f or t_D) are provided. In addition, the CQ times ($t_{start\text{-}CQ}$, $t_{end\text{-}CQ}$) and the intervention of MGI system time (t_{kG}) are also provided for VDEs. For mDs and ELMs, the starting and the ending time of the perturbation are reported. For L-H and H-L, the transition time is provided. Moreover, a reference time (t_{ref}) when the values of the plasma parameters are provided, is defined for each perturbation; in particular, VDEs reference time is defined based on the classification reported in section 2.1. Moreover, for VDEs and mDs, the time of the last L-H or H-L transition preceding the perturbation (if any) is given.

Table 1. Characteristic times for pulses containing VDEs, mDs, L-H/H-L and ELMs.

Time	**VDEs**	**mDs**	**L-H/H-L**	**ELMs**
Characteristic times	t_0, t_D, $t_{start\text{-}CQ}$, $t_{end\text{-}CQ}$, t_{kG} (if any)	t_0, t_f (or t_D), $t_{start\text{-}mD}$, $t_{end\text{-}mD}$	t_0, t_f (or t_D), t_{LH}, t_{HL}	t_0, t_f (or t_D), $t_{start\text{-}ELM}$, $t_{end\text{-}ELM}$
Reference time t_{ref}	Type1: t_D Type2: t_{kG} Type3: t_D	$t_{start\text{-}mD}$	L-H: t_{LH} H-L: t_{HL}	$t_{start\text{-}ELM}$
Last H-L transition (if any)	$t_{start\text{-}HL}$	$t_{start\text{-}HL}$	-	-
Last L-H transition (if any)	$t_{start\text{-}LH}$	$t_{start\text{-}LH}$	-	-

Accepted Manuscript

The study developed in Section 4 aims at characterizing the magnitude of the plasma displacement as function of the main plasma parameter variations and time derivatives during L-H and H-L transitions and ELMs for a prefixed plasma configuration. To this purpose, a database is built, which contains the maximum variation of the principal plasma equilibrium parameters (l_i, β_{pol} and Z_c) computed within a prefixed time window for each L-H/H-L transition and ELM, as reported in Table 2. To characterize the physical phenomenon, a time window lasting 200 ms around the transition time is considered both for slow and fast L-H/H-L transitions. The observed parameters have been averaged in the 100 ms before and after the transition time to remove noise effects. Instead, the maximum variations are computed during the ELM transient ($t_{start\text{-}ELM} \div t_{end\text{-}ELM}$) for ELMs. More than 300 JET discharges have been analyzed to populate the perturbation database, from specific experiments dedicated to L-H/H-L transition and H-mode scenario development in the presence/absence of impurities and in the presence/absence of pellets [24, 25]. Finally, about 60 discharges characterized by the following features have been selected:

- low and high triangularity
- plasma current ranging between 1.8 and 3 MA
- SN configurations.

Table 2: Plasma parameters provided in the experimental database for L-H/H-L transitions and ELMs

Plasma parameters	**L-H/H-L**	**ELMs**
Maximum variation of I_p,l_i, β_{pol}, Z_c	in the time window (t_{ref}-0.1s÷ t_{ref}+0.1s)	in the time window ($t_{start\text{-}ELM}$÷$t_{end\text{-}ELM}$)
Plasma configuration	at t_{ref}	at t_{ref}

The study developed in Section 5 aims at extrapolating to DEMO the trajectory of the plasma column, evaluating EM loads during a VDE and investigating the role of plasma transient perturbations in characterizing the VDE evolution. Thus, an inter-machine database of *DEMO relevant* VDEs and mDs has been built. For an adequate scaling to DEMO, ohmic discharges have been discarded from the database, and only mDs having a maximum plasma energy variation larger than 50% have been selected. The *DEMO relevant* conditions are identified by the q_{95} value, required to range between 3 and 4, and by a high value of the Greenwald fraction (f_{GRW}). As effect of the density peaking, the low collisionality and the fast particles in the turbulence stabilization, DEMO aims at f_{GRW} of about 1.2 [30]. Since such a value is not achievable in the present experimental reactors, the analysis has been restricted to a f_{GRW} larger than 0.7. In this work, the mean value of q_{95} evaluated in the last 500 ms before the perturbation has been considered to select the subset of *DEMO relevant* perturbations. Regarding the Greenwald fraction constraint, an in-depth analysis showed that most of disruptions are characterized by high variability of the Greenwald fraction signal in the last 500 ms before t_D. For this reason, its average or its value at t_D are not representative of the signal behaviour before the perturbation and the maximum value of the f_{GRW} ($f_{GRW\text{-}max}$) has been considered as *DEMO relevant* constraint, for both VDEs and mDs.

In the database provided in this study, the perturbations are featured by the values of I_p, l_i, β_{pol}, Z_c and R_c at the reference time and/or their variations (in a prefixed time window). In addition, information about powers from each additional heating system is provided. Finally, the triangularities and the elongation, the upper and lower X-point poloidal position, and the maximum variation of the radial separation of the two separatrices are given for discriminating among the different plasma configurations, together with the configuration at the reference time, as detailed in Table 3.

Table 3. Plasma parameters provided in the experimental database for VDEs and mDs

Plasma parameters	**VDEs**	**mDs**
I_p, f_{GW}, ΔZ_c *and* ΔR_c	value at t_{ref}	value at $t_{start\text{-}mD}$

Accepted Manuscript

I_p, li, β_{pol}	maximum variation in the time window $[t_{ref}\text{-}0.5s, t_{ref}]$	maximum variation in the time window $[t_{start\text{-}MD}, t_{end\text{-}MD}]$
q_{95}	mean value in the time window $[t_{ref}\text{-}0.5s, t_{ref}]$	mean value in the time window $[t_{ref}\text{ -}0.5s, t_{ref}]$
f_{GW}	maximum and mean values in the time window $[t_{ref}\text{-}0.5s, t_{ref}]$	maximum and mean values in the time window $[t_{start\text{-}mD}, t_{end\text{-}mD}]$
NBI, ECRH and ICRH power	value at t_{ref}	maximum value in the time window $[t_{start\text{-}mD}, t_{end\text{-}mD}]$
Plasma configuration	at t_{ref}	at t_{ref}
δ_u, δ_l	mean value in the time window $[t_{ref}\text{-}0.5s, t_{ref}]$	value at t_{ref} mean value in the time window $[t_{start\text{-}mD}, t_{end\text{-}mD}]$
k	mean value in the time window $[t_{ref}\text{-}0.5s, t_{ref}]$	value at t_{ref} mean value in the time window $[t_{start\text{-}mD}, t_{end\text{-}mD}]$
Upper and lower X-point vertical and radial position	value at t_{ref}	value at t_{ref} maximum variation in the time window $[t_{start\text{-}mD}, t_{end\text{-}mD}]$
Radial separation of the two separatrices	maximum variation in the time window $[t_{ref}\text{-}0.\ 5s, t_{ref}]$	maximum variation in the time window $[t_{start\text{-}mD}, t_{end\text{-}mD}]$

The resulting VDE databases contains six Type 1 and thirty Type 3 SN pulses for JET, where only 6 of them fulfil both the f_{GRW} and the q_{95} constrains; instead, six Type 1, thirty Type 2 and forty-five Type 3 VDEs are available for AUG: thirteen of them are *DEMO relevant*, seven of which are in QDN configuration.
The resulting mD database contains eighteen events for JET: five are *DEMO relevant*, one of which is QDN configuration; the AUG database resulted in four SN mDs: none of them is *DEMO relevant* because of the q_{95} constraint, which is always higher than the *DEMO relevant* upper limit.

4. Vertical displacement characterization during plasma transients

The database described in Table 2 has been used to characterize the plasma centroid vertical displacement. It contains L-H/H-L transitions and ELMs coming from experiments dedicated to H-mode scenario development [25]; in addition, the effect of the H-L transition on the VS has been investigated considering also Type 1 VDEs preceded by an H-L transition.
At this purpose, the plasma centroid vertical displacement during perturbations has been correlated to the variation of its internal parameters for JET slow (red points) and fast (blue points) L-H transitions. Figure 11 shows a similar correlation behaviour in terms of variation of β_{pol} and l_i with respect to the variation of the plasma centroid as discussed in [31], for both slow and fast L-H plasma perturbations. Indeed, using similar experimental observations, a set of plasma evolution simulations have been set up in [31], and discussed for the plasma position and shape control for ITER scenarios design strategy.

Accepted Manuscript

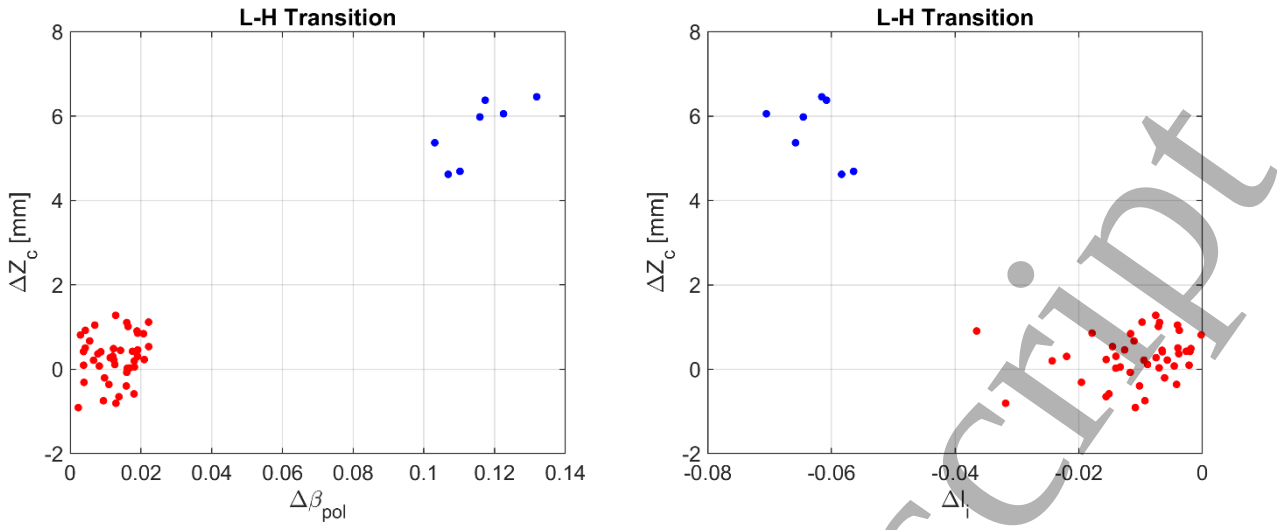

Figure 11. JET experimental data: Comparison between slow (red) and fast (blue) L-H transitions – plasma centroid vertical displacement versus variation of a) poloidal beta, b) internal inductance.

Figure 12 shows a correlation behaviour in terms of variation of β_{pol} and l_i with respect to the variation of the plasma centroid similar to the one discussed in [32] for ELMs plasma perturbations, and discussed for the most recent JET VS system. However, although the correlation in Figure 11 and Figure 12 do seem to find corroboration in [31, 32], further work would be needed to investigate the explicit parametric dependence between the analysed variables.

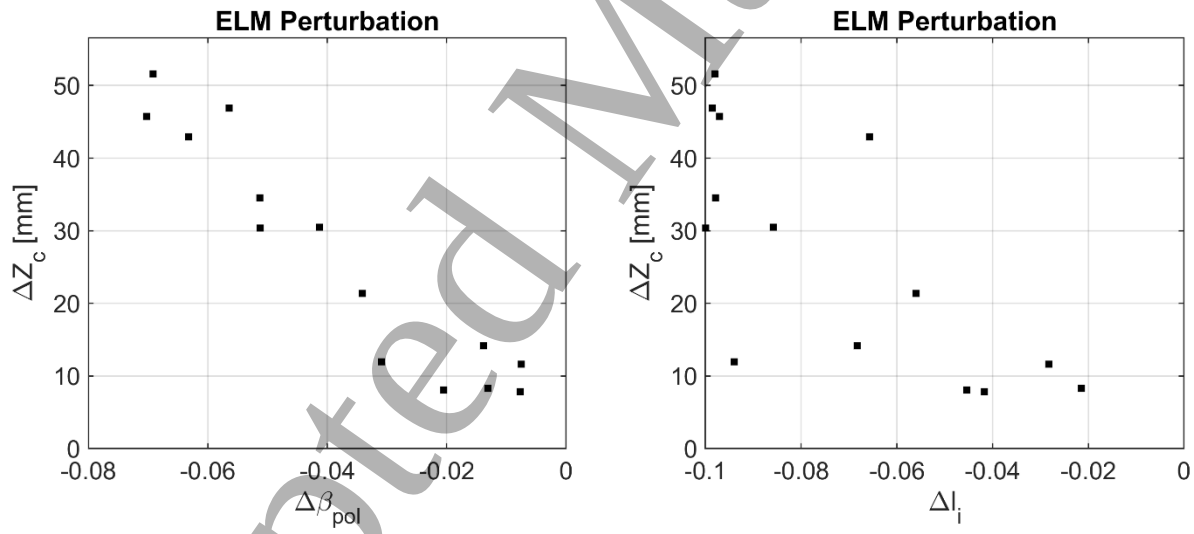

Figure 12. JET experimental data: ELMs effects on plasma centroid vertical displacement versus variation of a) poloidal beta and b) internal inductance.

A similar behavior has been obtained also for H-L transitions, as shown in Figure 13.

Accepted Manuscript

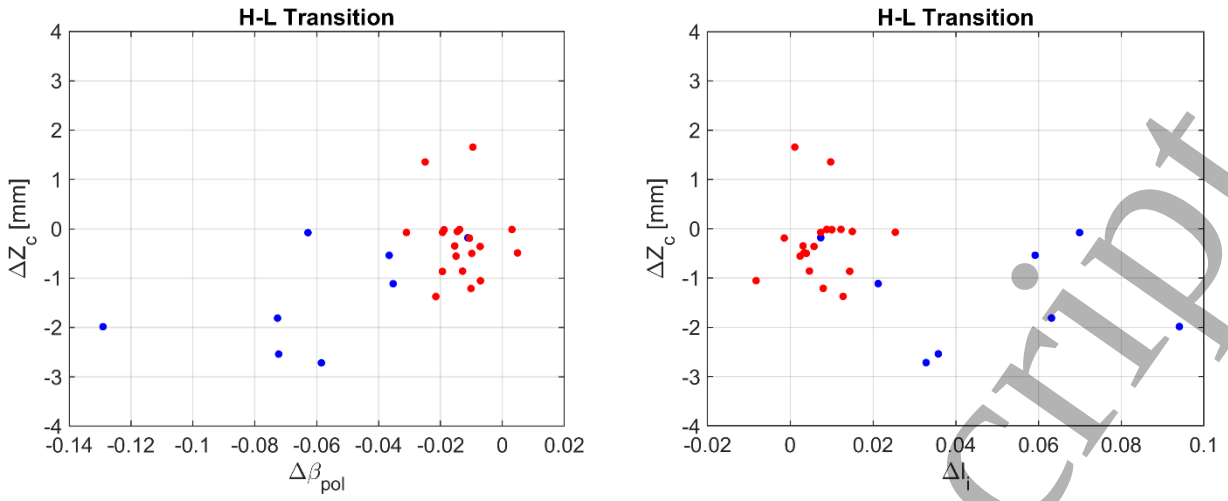

Figure 13. JET experimental data: Comparison between slow (red) and fast (blue) H-L transitions – plasma centroid vertical displacement versus variation of a) poloidal beta and b) internal inductance.

The investigation of such a behavior has been deepened by correlating the plasma centroid vertical displacement also with the global time derivative of the internal parameters, evaluated in the considered observation time window (200ms for L-H/H-L transition and $t_{start\text{-}ELM} \div t_{end\text{-}ELM}$ for ELMs).

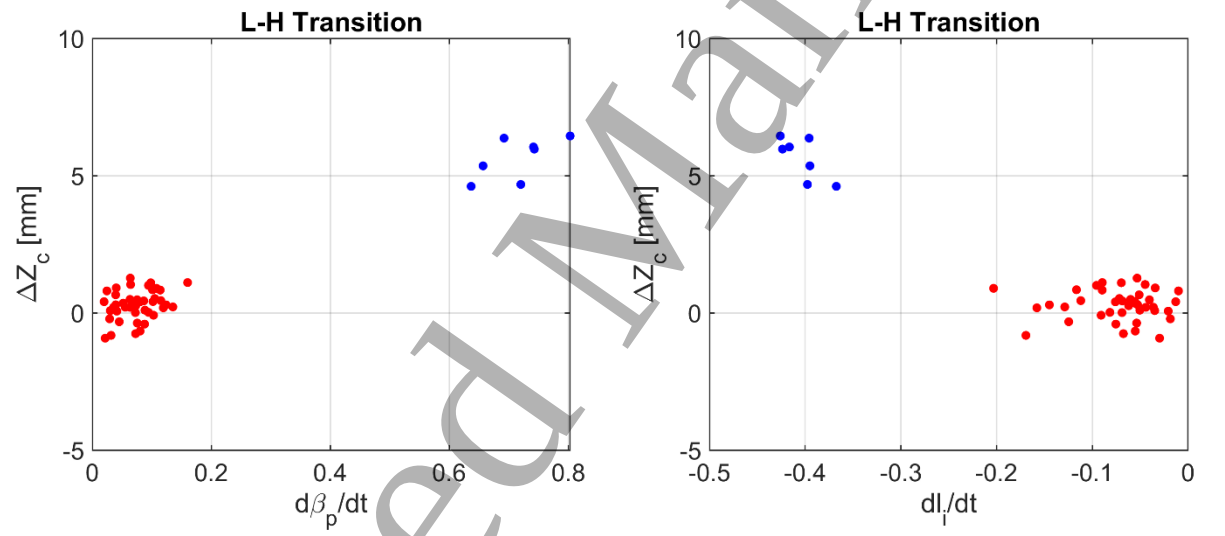

Figure 14. JET experimental data: Comparison between slow (red) and fast (blue) L-H transitions – plasma centroid vertical displacement versus a) poloidal beta time derivative and b) internal inductance time derivative.

Accepted Manuscript

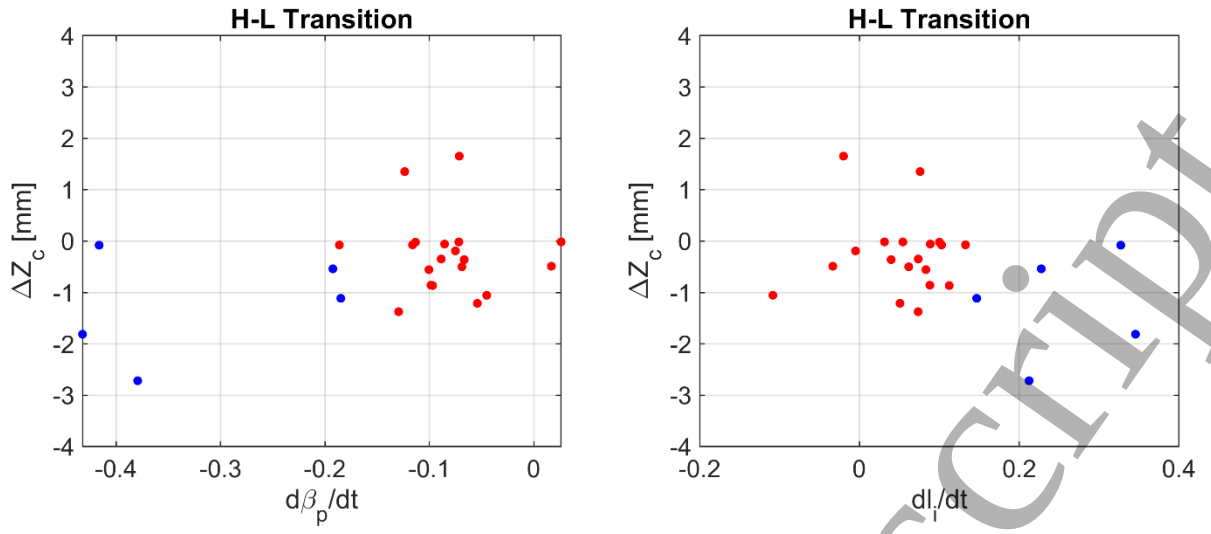

Figure 15. JET experimental data: Comparison between slow (red) and fast (blue) H-L transitions – plasma centroid vertical displacement versus a) poloidal beta time derivative and b) internal inductance time derivative.

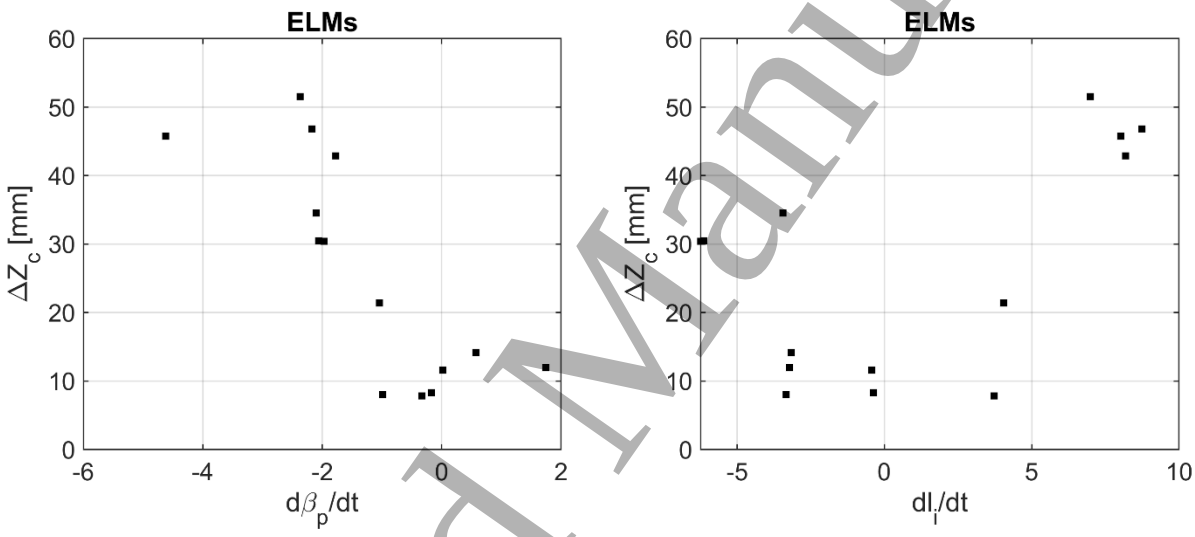

Figure 16. JET experimental data: ELMs effects on plasma centroid vertical displacement versus a) poloidal beta time derivative and b) internal inductance time derivative.

Figure 14, Figure 15, and Figure 16 explain why slow transitions and fast transitions are characterized by similar values of the vertical displacement of the plasma column even in the presence of very different variations of the plasma internal parameters. This effect is not caused by the VS systems, which is able to feedback to zero the vertical velocity of the plasma centroid with a duty cycle lasting 50 μs but by the plasma position control, which feedbacks the plasma vertical position every 2 ms. ELMs are indeed much faster perturbations than L-H and H-L transitions and their effect in terms of perturbation velocity and vertical displacement of the plasma column is affected by the VS system [32].

To investigate how the observed behavior changes if a VDE follows the L-H/H-L transition, five Type 1 VDEs discharges, contained in the VDE database described in Section 3.5, have been added to the study. In Figure 17, the internal parameters variation at the L-H transition time of the extended database are shown, where the black markers correspond to the new hot VDEs.

Accepted Manuscript

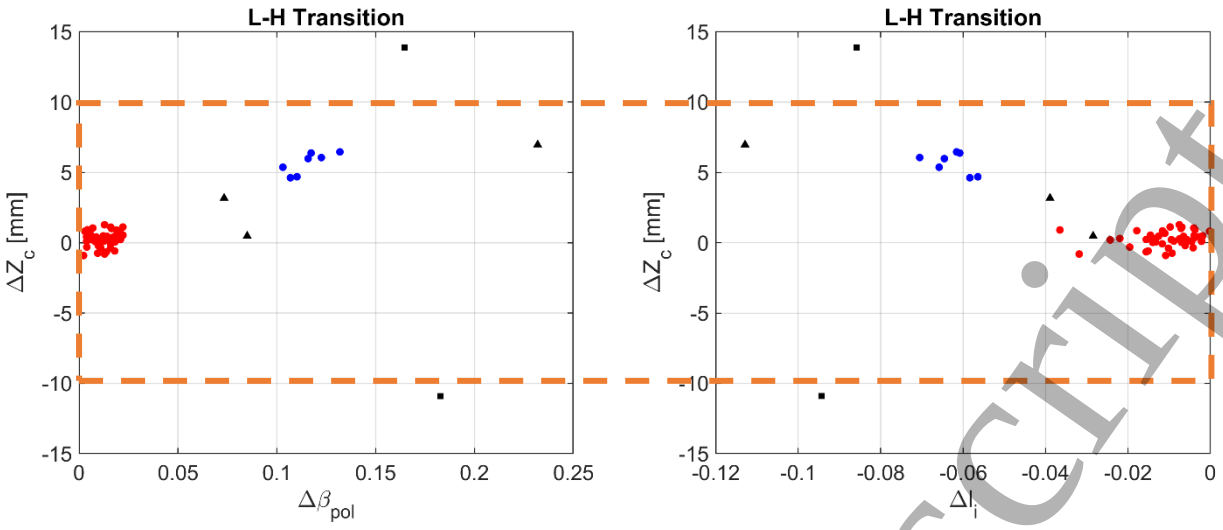

Figure 17. Comparison between the L-H transitions in Figure 11 (blue and red colored points) and VDEs (black colored points) selected from the experimental database detailed in Section 3.5: plasma centroid vertical displacement versus variation of a) poloidal beta, and b) internal inductance.

In Figure 17, the new discharges have been added to those in figure 11 and marked with a square if an initial strong MHD activity is observed before the L-H transition and with a triangle if not. The VDEs marked with a triangle follow the same behavior shown in Figure 11 (remaining inside the region bordered by the orange dashed line, $|\Delta Z_c| \leq 10\ mm$). For those marked with a square, a larger variation ($|\Delta Z_c| > 10\ mm$) of the plasma vertical position is present, falling outside the orange bordered region.

5. MAXFEA reconstruction of plasma dynamic behaviour during plasma perturbation phases and scaling to DEMO

In this section, the plasma final position and the EM loads following a VDE are predicted in DEMO baseline geometries. 2D numerical simulations on designed discharges characterised by transient plasma perturbations and ended in VDEs are performed using MAXFEA code. It should be noted that due to the length of the paper and difficulties on finding experimental ELMs plasma perturbations combined with VDEs in DEMO relevant conditions to be accordingly scaled, only some of the plasma perturbations presented in the previous sections will be discussed here. The plasma magnetic flux map of collected experimental transient perturbations is used as guideline for the investigation of the plasma behaviour in DEMO scenarios. In particular, the following simulation starting from experimental data are presented: a Type 1 VDE preceded by a H-L transition referring to JET pulse #91991; a Type 3 VDE preceded by a mD, referring to JET pulse #92132; Type 1 and Type 3 VDEs in SN DEMO configuration, referring to JET pulse #92132; a Type 1 VDE preceded by a plasma mD in QDN configuration, referring to JET pulse #68805; a Type 1 VDE in QDN configuration preceded by a H-L transition and mD, referring to AUG pulse #32120; Type 3 VDE analysis in DN and QDN in DEMO2020 scenario, scaling from JET pulse #68805.

5.1 JET H-L transition followed by Type 1 VDE

The JET Type 1 VDE discharge #91991, occurring at flat-top of plasma current in *DEMO relevant* condition has been simulated by MAXFEA code with an event characterized by the same β_{pol} and *li* variations during the H-L transition. The event has been simulated in MAXFEA starting from the same magnetic configuration of the #91991 discharge just before the TQ up to the end of the VDE. Figure 18 reports the experimental time evolution of D_α, poloidal beta β_{pol}, plasma centroid vertical position Z_c, and NBI heating power (P_{NBI}). The vertical dashed line indicates the H-L transition time, detected as described in Section 3.3. The CREATE-NL

Accepted Manuscript

[13] equilibrium parameters at prefixed times are given as inputs to MAXFEA simulation and are reported in Table 4. The resulting MAXFEA equilibrium at H-L transition time is shown in Figure 19.

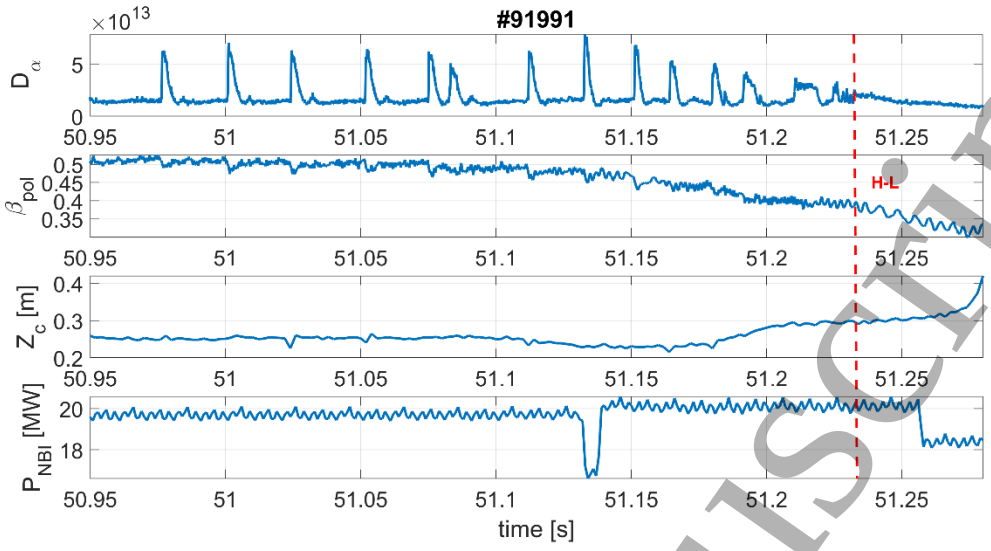

Figure 18. JET-ILW pulse #91991: Experimental time evolution of D_α, poloidal beta β_{pol}, plasma centroid vertical position Z_c, averaged electron density n_e, and additional heating power (P_{NBI}).

Table 4: JET-ILW pulse #91991 – CREATE-NL equilibrium parameters at prefixed times.

	t[s]	β_{pol}	li	I_p [MA]	Z_c [m]	R_c [m]
L-H transition	49	0.038	1.025	2.428	0.237	2.88
Stable H-Mode	49.385	0.25	0.962	2.498	0.239	2.897
H-L transition	51.23	0.286	0.838	2.467	0.26	2.873
Last X-point status	51.287	0.231	0.88	2.442	0.287	2.829
Thermal Quench start	51.287					
Current Quench start	51.299					
Current Quench end	51.345					

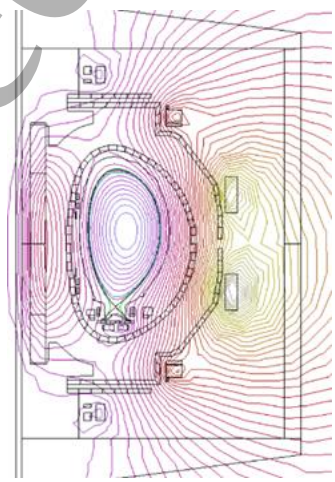

Figure 19. JET-ILW pulse #91991: MAXFEA equilibrium at H-L transition time.

It should be noted that in a time window of 50 ms during the H-L transition:

- β_{pol} decreases from 0.286 to 0.231 and li increases from 0.838 to 0.880;

Accepted Manuscript

- Z_c increases of 3 cm and R_c decreases of 4 cm.

Thus, the pulse #91991 shows a critical condition that could lead a VDE. Indeed, a first sawtooth crashed and triggered a 3/2 NTM instability, that slowly locked and consequently promoted a VDE, according to daily JET physical report. During the Thermal Quench (TQ), a good agreement between experimental data and MAXFEA simulation phase has been found in terms of variation of plasma centroid position as shown in Figure 20.

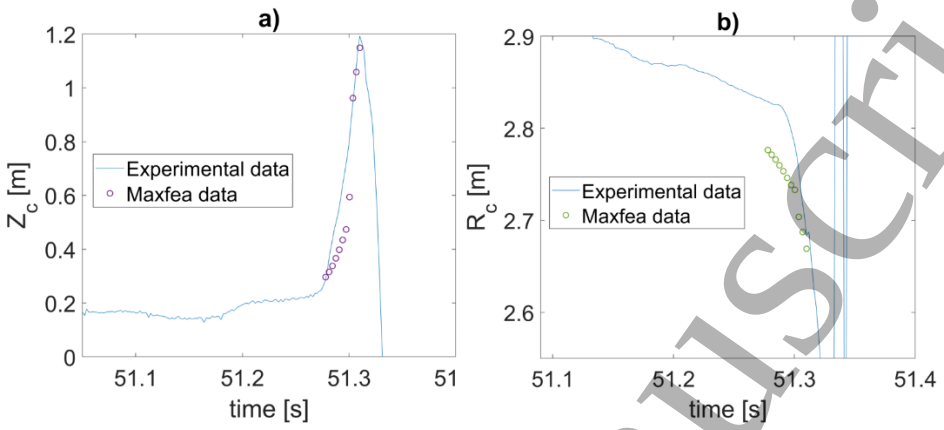

Figure 20. JET-ILW pulse #91991: MAXFEA simulated a) vertical coordinate Z_c (purple circle) and b) radial coordinate R_c (green circle) of plasma centroid during the TQ phase compared with respect to their own experimental signals (blue lines).

Electromagnetic vertical loads, eddy, and halo currents on VV have been also calculated during the simulated event. In Figure 21, the vertical component of the MAXFEA simulated EM loads due to halo and eddy currents are reported in blue and red respectively, whereas the total vertical force is reported in yellow; the simulated plasma current is reported in purple. A peak vertical force F_Z~800 kN calculated by MAXFEA is in the same order of magnitude of the experimental one.

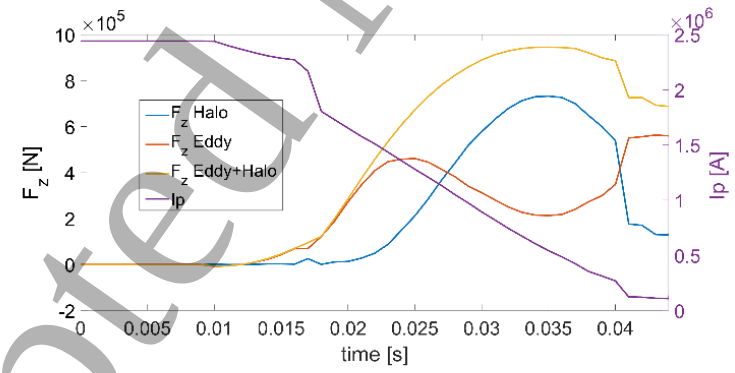

Figure 21. JET-ILW pulse #91991. Vertical forces (halo and eddy) simulated by MAXFEA during a Type 1 VDE (TQ+CQ ~ 40 ms). The blue and red lines indicate the forces due to halo and eddy current respectively, whereas the total force is reported in yellow. The purple line reports the simulated plasma current.

Figure 22 reports the currents: halo in green, eddy on the upper VV in red, eddy on the lower VV in orange, whereas the eddy current evaluated on the entire VV is reported in blue. The induced currents are about 60% of plasma current I_p (in purple) during TQ and the following CQ, as regularly observed at JET.

Accepted Manuscript

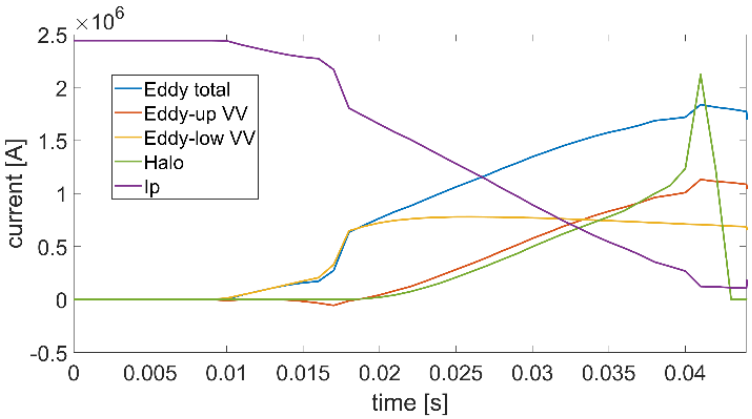

Figure 22. JET-ILW pulse #91991: MAXFEA simulated currents. The plasma current (purple line) during a Type 1 VDE (TQ+CQ ~ 40 ms), the halo current is reported in green, the eddy current on the upper and lower VV are reported in red and orange respectively, whereas the one on the entire VV is reported in blue.

Finally, a disruption event similar to JET pulse #91991 has been modelled in DEMO to reproduce a VDE following an H-L transition. The CQ duration has been opportunely scaled to DEMO following what reported in [33]. First, standard SN equilibrium has been reproduced by using 2017 baseline geometrical configuration and reported in Figure 23. The H-L plasma event (described as a glitch of poloidal beta) triggers the VDE and the plasma moves until it hits the wall. When the boundary safety factor q drops below 2, the thermal quench occurs, lasting 4 ms, with a plasma current I_p spike ≈ 5% [20]. Immediately after, linear current quench takes place, assumed to last 74 ms [20]. The VDE behaviour, in terms of plasma trajectory depicted by the radial and vertical plasma centroid position (R_c and Z_c respectively) calculated by MAXFEA is shown in Figure 24. It should be noted that, the results are quite similar to the one discussed in [20] obtained by CARMA0NL and CREATE-L codes.

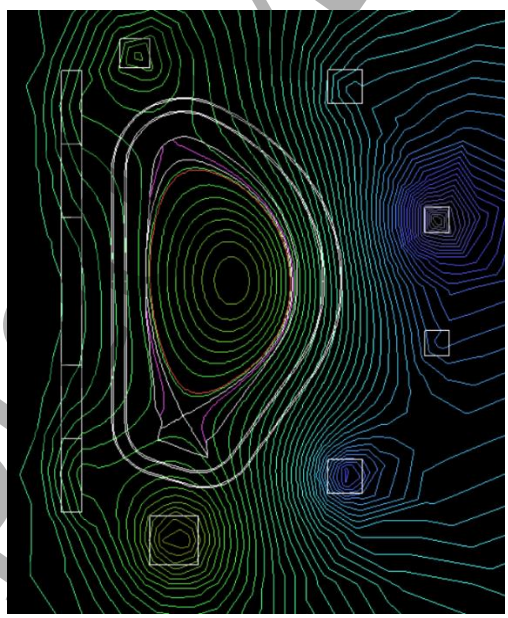

Figure 23. DEMO SN configuration with 2017 baseline geometry (updated to 2019) realized in MAXFEA code suite. [19].

Accepted Manuscript

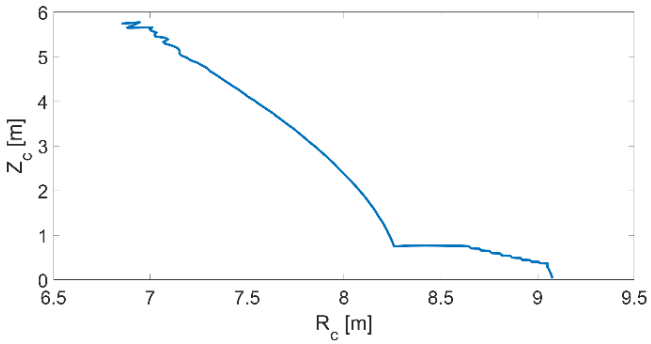

Figure 24. MAXFEA simulation of the plasma barycentre trajectory during a VDE scaled by JET pulse #91991 to SN DEMO baseline geometry.

In addition, halo and eddy currents and the corresponding EM loads have been computed. The electromagnetic vertical forces on VV are reported in Figure 25, together with the simulated plasma current. The currents are shown in Figure 26: halo in green, eddy on the upper VV in red, eddy on the lower VV in orange, whereas the halo current on the entire VV is reported in blue. A vertical force of ~25 MN has been found.

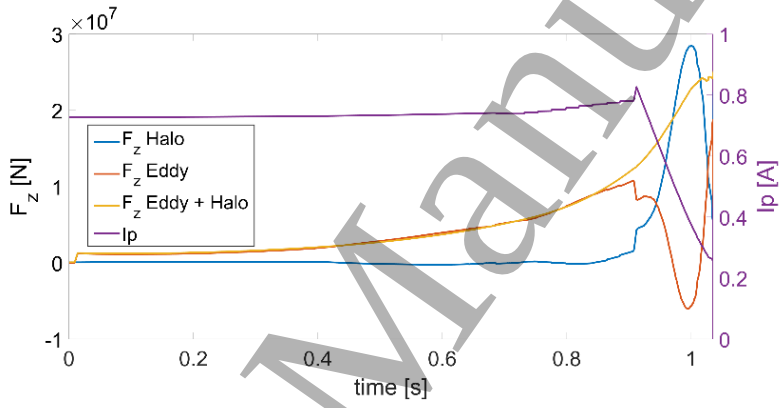

Figure 25. Vertical forces (halo and eddy) simulated by MAXFEA for SN 2017 DEMO baseline scaled by JET pulse #91991. The blue and red lines indicate the forces due to halo and eddy current respectively, the total force is reported in yellow. The purple line reports the simulated plasma current.

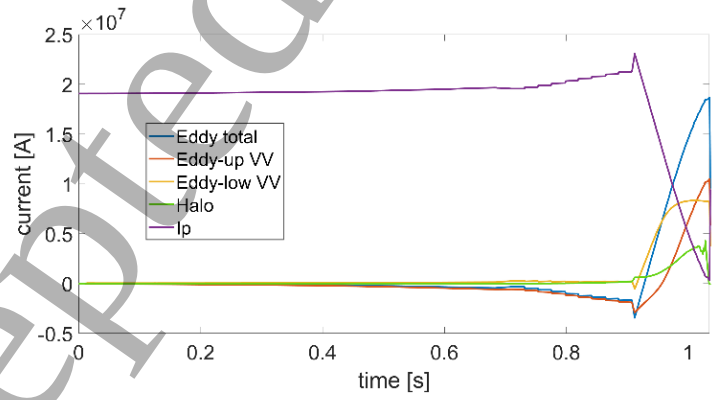

Figure 26. MAXFEA simulated currents for SN 2017 DEMO baseline scaled by JET pulse #91991. The halo current is reported in green, the eddy currents on the upper and lower VV are reported in red and orange respectively, whereas the one on the entire VV is reported in blue. The purple line reports the simulated plasma current.

5.2 JET mD followed by Type 3 VDE

The JET pulse #92132 is characterized by a minor disruption occurred in DEMO relevant conditions (i.e., f_{gw}>0.7 and 3<q_{95}<4) at the flat-top and ended with a MD followed by a downwards VDE (Type 3 VDE). The

Accepted Manuscript

simulations results show a good agreement with experimental data in terms of displacement of plasma centroid during the TQ phase (see Figure 27 a) and b)).

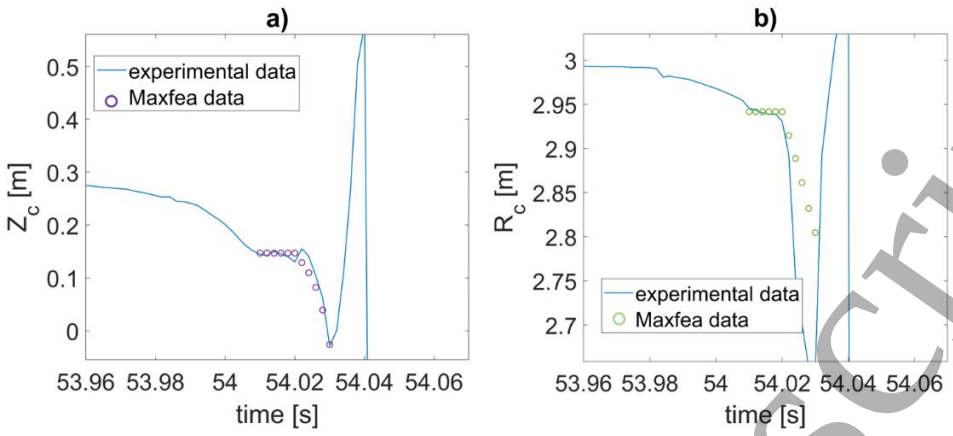

Figure 27. JET-ILW pulse #92132: MAXFEA simulated variation of the a) vertical coordinate Z_c (purple circle) and b) radial coordinate R_c (green circle) of plasma centroid during the TQ phase compared with respect to their own experimental signals (blue lines).

5.3 Type 1 and Type 3 VDE analysis considering DEMO2017.1c scenario

A set of disruptions following plasma perturbations adapted to DEMO conditions has been simulated by means of MAXFEA code. Both MDs and hot VDEs can follow a plasma perturbation. Usually, MDs are more frequent but also hot VDEs can happen, often when the plasma is perturbated far from the neutral point or when the vertical position controller actuator is working near its limit. The MAXFEA simulation of JET discharge #92132 has been used as guideline in the investigation of plasma behavior during a set of possible MDs and hot VDEs, both occurring at start of flat-top phase (SOF) and at end of flat-top (EOF) phase [19].
The DEMO 2017 reference geometry [16] and the demo2017.1c scenario [33] have been used for these simulations. The main simulation parameters are adopted with the criteria shown in [33]. Since EM loads due to eddy and halo currents in fast and slow plasma disruptions are among the four load categories considered in the design of the DEMO components [33], two different CQ durations, ~74 ms and ~300 ms are considered, as fast and slow respectively. The sequence of actions adopted to describe the different disruptions in MAXFEA are the following:

- Major Disruptions (MD), modelled with:
  - TQ occurring 10 ms after the start of simulation;
  - Loss of position control after the TQ;
  - Halo currents when plasma touches the wall;
  - Different CQ durations (~74 and ~300 ms).
- Upward VDE (UVDE) modelled with:
  - Destabilizing kick 10 ms after the start of simulation to simulate the loss of position control;
  - Halo currents when plasma touches the wall;
  - TQ at a given critical safety factor (q_{95}=2);
  - Different CQ durations (~74 and ~300 ms).

Note that, MAXFEA code treats the halo currents with a very first-principle method. Since MAXFEA assumes that plasma evolves with a quasi-static approximation, the plasma is always in a state of mechanical equilibrium and the global halo currents force is estimated from the force balance. The total amount of halo current is estimated starting from the force balance and an input parameter related to the halo region width.
Table 5 and Table 6 summarize the results in terms of halo currents and EM loads for disruptions occurring at the SOF and at EOF phase respectively. The first column lists the simulated events (MD and UVDE) for the

Accepted Manuscript

two different CQ durations, identified by the subscript *F* (fast) or *S* (slow). The second column reports the variation of plasma vertical position ΔZ_c at the disruption time. The third column reports the maximum value of the halo currents ($I_{halo\text{-}max}$). The fourth column reports the maximum value of the vertical forces on the VV. The fifth column reports the plasma current (I_p) evaluated at the disruption time. The sixth column reports the halo maximum axisymmetric index [33], evaluated as: $I_{halo-max}\ /I_p(t_D)$.

Table 5. Main results of MAXFEA simulation of reference SOF disruptions for the DEMO 2017 design.

Event	$\Delta Z_c(t_D)$ [m]	$I_{halo\text{-}max}$ [MA]	$F_{z\text{-}max}$ [MN]	$I_p(t_D)$ [MA]	Axisym. max halo
MD_F	-0.11	2.6	4.2	19.07	≈0.15
MD_S*	-0.11	-	-	19.07	-
$UVDE_F$	0.12	2.3	31.4	19.33	≈0.15
$UVDE_S$	0.09	3.5	48.4	19.33	≈0.20

* for this case, it was not possible to simulate the CQ for all its duration.

Table 6. Main results of MAXFEA simulation of reference EOF disruptions for the DEMO 2017 design.

Event	$\Delta Z_c(t_D)$ [m]	$I_{halo\text{-}max}$ [MA]	$F_{z\text{-}max}$ [MN]	$I_p(t_D)$ [MA]	Axisim. max halo
MD_F	-0.07	2.3	5.9	19.07	≈0.15
MD_S	-0.07	3.7	27	19.07	≈0.20
$UVDE_F$	0.15	2.4	40.7	19.33	≈0.15
$UVDE_S$	0.12	3.7	61.7	19.33	≈0.20

It should be noted that the worst case, in terms of higher halo current and vertical force on the VV, results in the UVDE at EOF phase by considering a current quench duration of 300 ms ($UVDE_S$), with $I_{halo\text{-}max}$≈3.7 MA and $F_{z\text{-}max}$≈61.7 MN.

In Figure 28 a-d, the UVDE worst case for DEMO 2017 design is summarized in terms of MAXFEA simulated currents, EM loads on the VV, last closed flux surfaces (LFCSs) during the disruption and limiter contact point evolution.

Accepted Manuscript

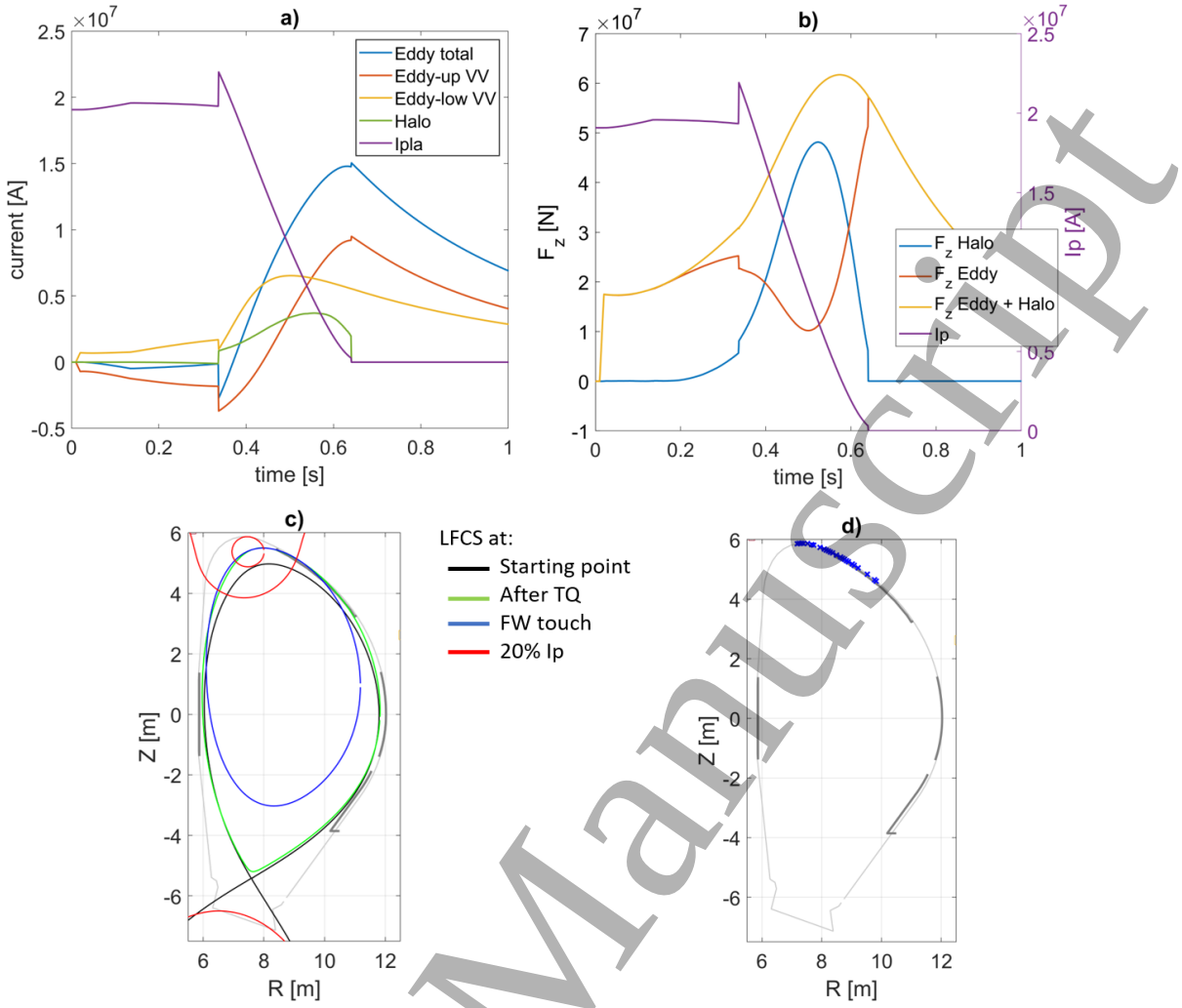

Figure 28. MAXFEA DEMO 2017 UVDEs simulation results: a) halo and eddy currents and plasma current, b) EM loads on VV, c) LFCS shape: at starting point of disruption (in black), immediately after Thermal Quench (in green), when plasma touches the First Wall (blue) and for a plasma with 20% of the starting current (red), d) limiter contact points (blue x-markers).

5.4 JET Quasi Double Null plasma mD followed by a Type 1 VDE

A preliminary study on a QDN perturbation has also been carried out, focused on an experimental mD at high density (f_{GRW}>0.7). This study is based on the QDN C-wall JET discharge #68805 occurred in the time window (46.720÷46.770), already discussed in Section 3.4. The considered time window is characterized by a mD perturbation (see Figure 29), recovered by the control system triggering a soft stop. The plasma is heated with auxiliary power system and reaches $f_{GW,max}$=1.3, q_{95} =6.1 and a maximum variation of plasma energy of about 31% (see W_{mhd} evolution described by the red line in Figure 29). Although some constrains do not fit the DEMO requirements, pulse #68805 was the only one having a transient plasma perturbation occurring in QDN configuration.

Accepted Manuscript

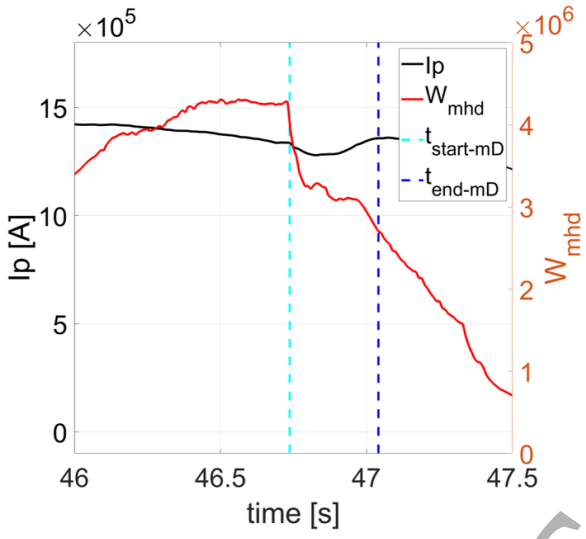

Figure 29. JET pulse # 68805: minor disruption evolution. The plasma current (black line) gap between 46.720 s and 46.770 s is combined with a collapse of plasma energy W_{mhd} (red line). Cyan and blue dashed vertical lines are the mD starting and the ending times respectively.

In this study, a first comparison between an experimental and simulation mD is performed, then a VDE is triggered as described below.

The QDN reference configuration has been simulated by CREATE-NL at 46.6 s, resulting in: I_p = 1.354 MA, β_{pol}=1.76, l_i=0.88; the distance of the secondary inactive null from the separatrix is equal to 0.38 m as also reproduced by MAXFEA code (see Figure 30). The minor disruption has been modelled as following:

- ✓ t_{start}= 46.7 s
- ✓ $t_{mD\text{-}start} = t_{start} + 0.02s$
- ✓ a linear variation of experimental β_{pol} and l_i is imposed in the mD time window (46.720÷46.770) s

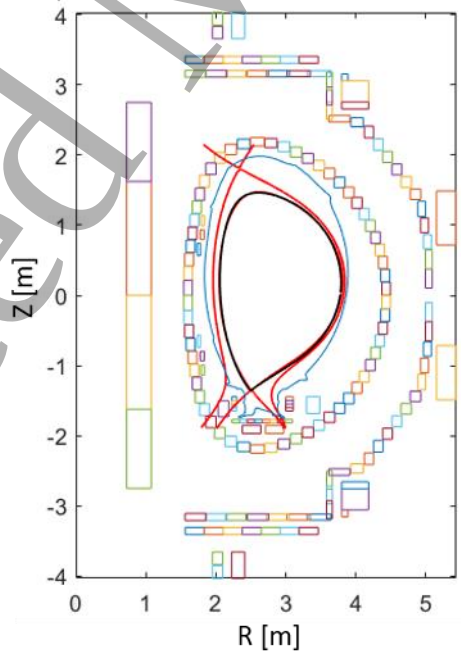

Figure 30. JET QDN pulse #68805 discharge @ 46.6s: CREATE-NL plasma equilibrium (red solid line) vs the MAXFEA one (black solid line).

Accepted Manuscript

As shown in Figure 31, a good agreement between the experimental and simulated data has been obtained during the mD phase (between 46.720 s and 46.770 s) in terms of plasma centroid shift in vertical and radial direction (Z_c and R_c coordinates).

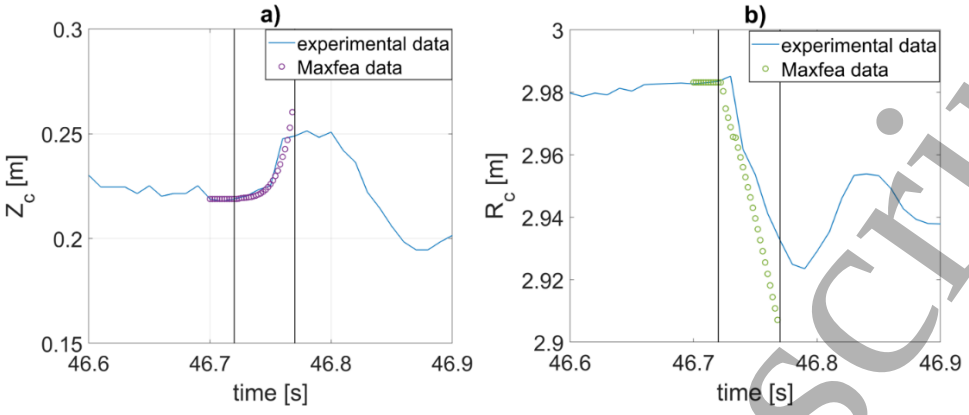

Figure 31. JET QDN pulse #68805: experimental evolution (blue solid line) vs the MAXFEA simulated ones (purple circles) of plasma centroid vertical and radial position (a and b subplot respectively) during the mD phase.

Differently from the experimental discharge, where the mD has been recovered by control system, a Type 1 VDE triggered by the mD is simulated in this study. The VDE is based on the previous studies reported in section 5.1; moreover, it considers the differences between the C-wall and ILW discussed in [34], and shown in Figure 32 where the disruption rate is evaluated as a function of the ratio between the CQ time window in ms (τ_{CQ}) and plasma surface *S*. The duration of the CQ is obtained considering *S* as equal to the area of the plasma poloidal section just before the event occurrence (see Figure 32). The VDE has been modelled as following:

- TQ modelled as β_{pol} drop in 1ms when the plasma approaches $q_{95} \approx 3$;
- Halo currents after TQ: 25% of I_p before the minor disruption;
- CQ of 11ms just after the TQ. Assuming: $\tau_{CQ}/S \approx 3$, as in the most frequent case for C-wall (see Figure 32), and S~3.6 m^2 (evaluated on the discharge #68805 before the mD occurrence), τ_{CQ} results in about 11 ms.

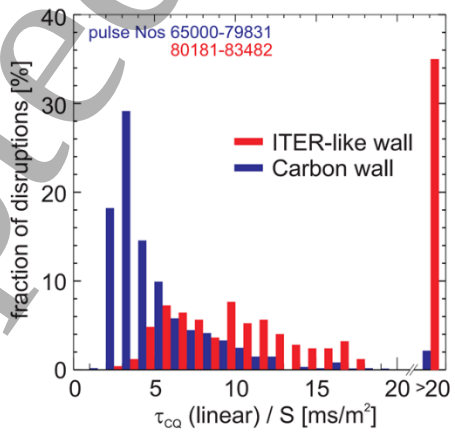

Figure 32. Disruption rate distribution as function of the ratio between the CQ time window τ_{CQ} [ms] and plasma surface *S* [m^2], for JET C-wall (blue) and ILW (red) [34].

The simulation results in QDN for JET pulse #68805 are shown in Figure 33, where subplot a) reports the plasma separatrix at VDE starting point (red solid line), together with the trajectory of the plasma centroid

Accepted Manuscript

during the VDE phase (solid blue line). Subplot b) reports the halo (orange) and eddy (yellow) currents behaviour together with the simulated plasma current (in purple). Subplot c) reports the electromagnetic vertical forces on VV due to halo current (in orange), eddy current (blue) and their sum (yellow). The purple line is the simulated plasma current. The simulated EM loads and the halo current contributions are in good agreement with VDE experimental conditions discussed in [34].

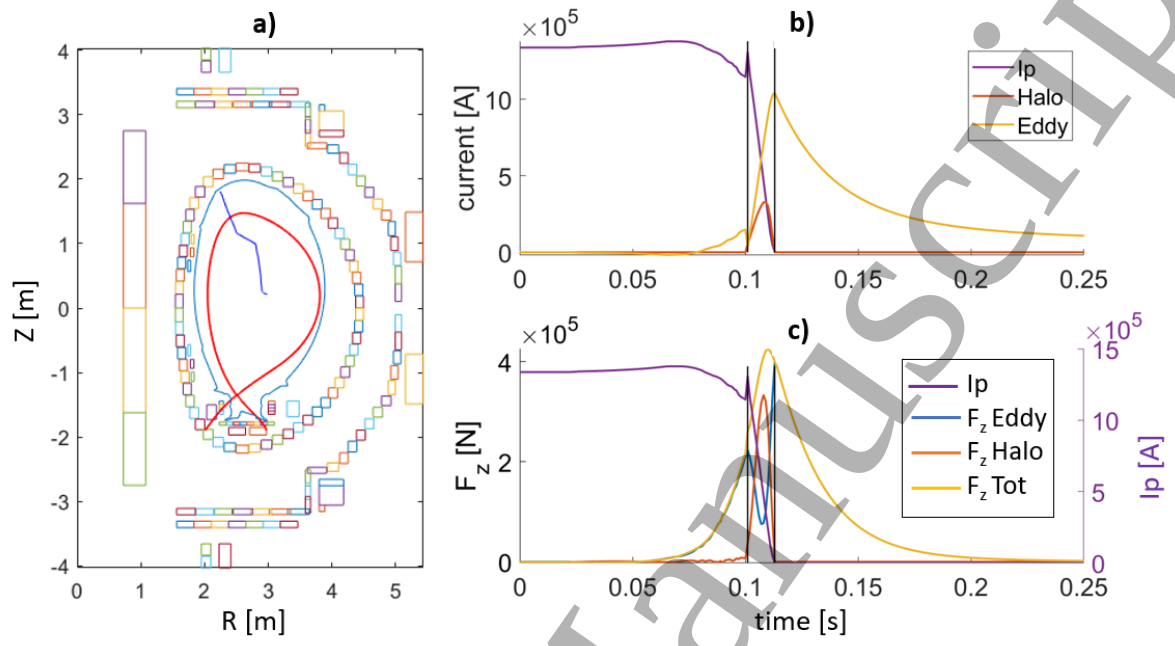

Figure 33. MAXFEA QDN simulation referred to JET pulse #68805: a) plasma separatrix at VDE starting point (red solid line), centroid plasma trajectory during VDE (solid blue line); on the right subplots, the purple line reports the simulated plasma current, moreover, subplot b) reports the currents, halo (red line) and eddy (yellow line); subplot c) reports the simulated EM loads on VV: eddy (blue), halo (red) and the total (yellow) vertical forces.

5.5 AUG mD followed by a QDN Type 1 VDE

The AUG Type 1 VDE discharge #32120 occurs at flat-top of plasma current in QDN configuration and DEMO relevant condition. The VDE occurs at 5.719s, about 160 ms after the HL transition.

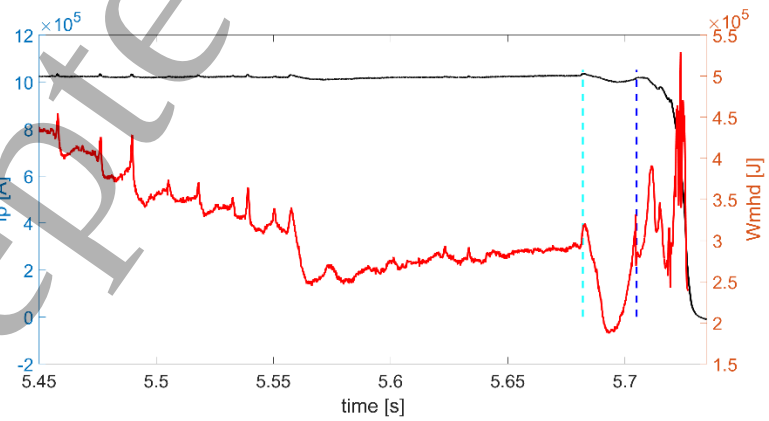

Figure 34. AUG pulse #32120: Type 1 VDE discharge in QDN configuration. The plasma current (black line) gap between 5.681s s and 5.702 s is combined with a collapse of plasma energy W_{mhd} (red line). Cyan and blue dashed vertical lines are the mD starting and the ending times respectively.

Accepted Manuscript

Looking at the ending phase of the shot, a minor disruption occurs between 5.681s and 5.702 (see cyan and blue dashed lines in Figure 34, respectively), with a maximum variation of plasma energy of about 41% (see red line in figure 34). In the last 150 ms, the pulse is heated with auxiliary power system and reaches a f_{GW} larger than 0.89 with q_{95} =6.1.

Because of the mD, the plasma becomes vertically unstable, and the control system tries to move the plasma to its equilibrium position, as reported by the evolution of the vertical position Z_c signal in Figure 35b between the cyan and the blue vertical lines. In the time window between the blue and red vertical lines, the control system fails to recover the plasma and it starts to move upward. In this phase, there is not a great change in the plasma current until conditions for a rapid TQ occurs at 5.719 s (red vertical line in Figure 35a) and plasma disrupts. The ensuing increase in plasma resistivity produces the CQ and the current is lost in about 13 ms.

An AUG MAXFEA model has been set-up including all the main passive structures (Figure 36), and the VDE phase has been simulated with the following strategy:

- Equilibrium at 5.702 has been reproduced (see Figure 37) and used as a starting point for the simulation of the plasma evolution.
- A destabilizing kick is applied by means of a dummy coil at the beginning of the simulation to force the plasma up-ward movement.
- During the first phase of the vertical displacement, from 5.702 s to 5.719 s (TQ starting time) the evolution of the simulated plasma current model is imposed to follow the experimental one (Figure 38).
- At 5.719 s the TQ is imposed by a β_{pol} drop in 1 ms.
- The CQ phase begins immediately after the TQ.

In order to guarantee the force balance and the convergence of the simulation during the CQ phase, the presence of the halo current is assumed by means of the MAXFEA halo module. Since in the halo module it is no longer possible to directly impose the evolution of the plasma current, the CQ is simulated imposing a certain negative voltage on plasma to reproduce a similar current evolution (see Figure 38).

Although divergent behaviours are evident between simulated and experimental data at CQ starting time (see Figure 39), the proposed procedure could give useful indications on plasma centroid movement in vertical and radial direction to be taken into account during VDE analysis, considering all the possible sources of discrepancies due to the model simplifications introduced for MAXFEA code simulation and discussed in [19].

Accepted Manuscript

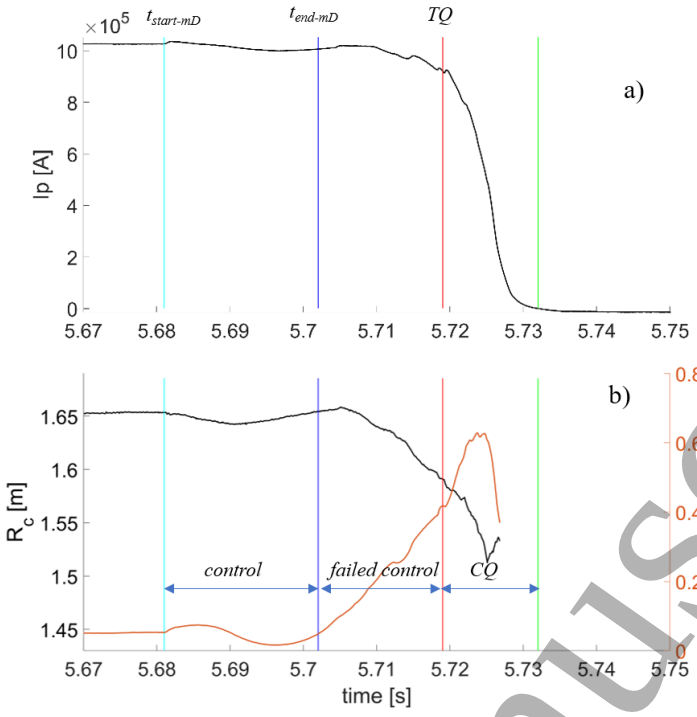

Figure 35. AUG pulse #32120: Plasma current and plasma centroid evolutions during the ending phase of the shot. a) Plasma current b) R_c (black) and Z_c (orange) evolutions.

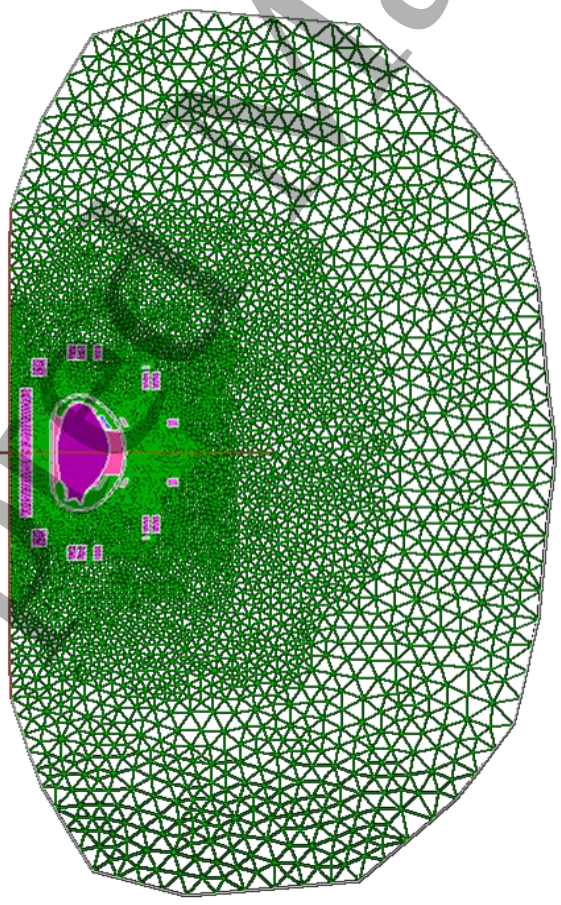

Figure 36. MAXFEA AUG model overview

Accepted Manuscript

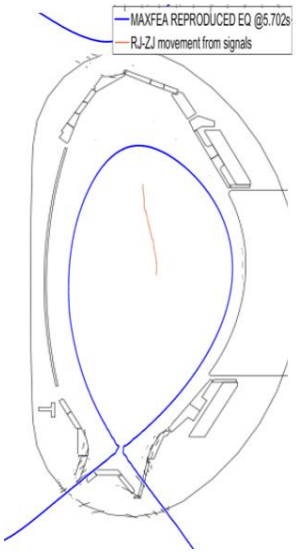

Figure 37. Equilibrium @5.702 (VDE start) reproduced by means of MAXFEA code: LCFS (blue) and R_c-Z_c movement during VDE from signals (red).

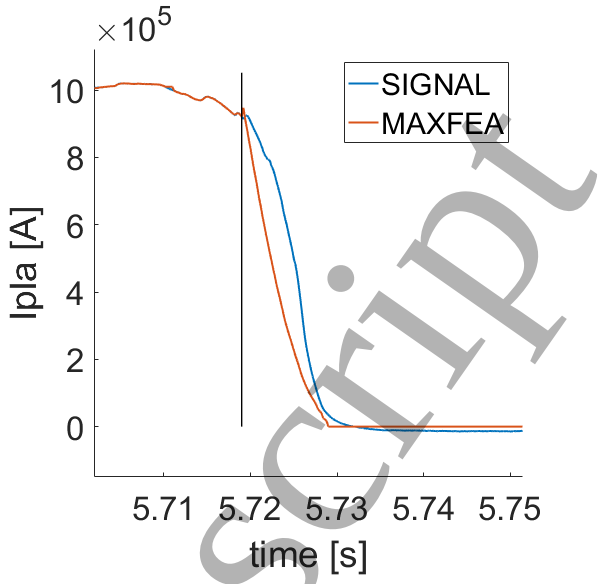

Figure 38. Plasma current evolution in time: experimental signal (blue) and MAXFEA simulation (red).

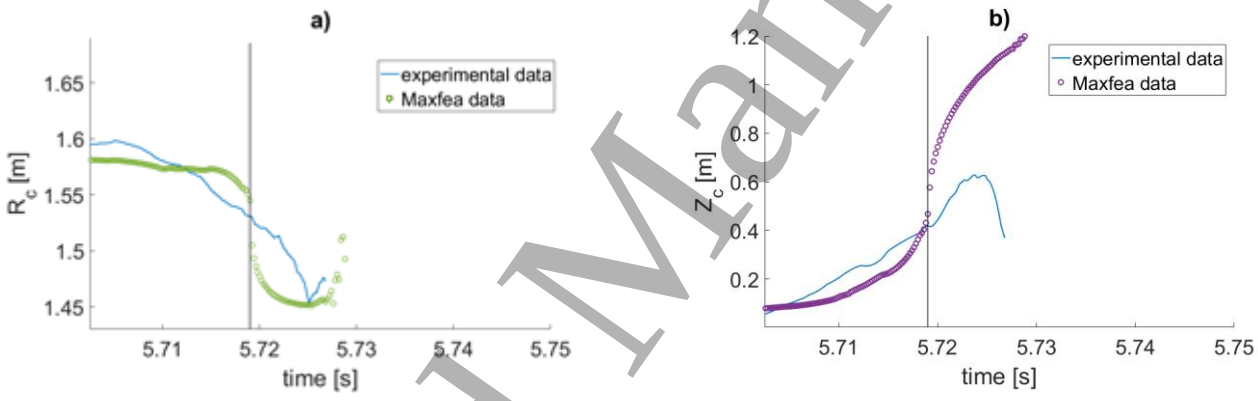

Figure 39. AUG pulse #32120: experimental evolution (blue solid line) vs the MAXFEA simulated ones (circles) of plasma centroid vertical and radial position (a) and b) subplot respectively) during the VDE phase.

5.6 DN Type 3 VDE analysis in DEMO2020 scenario

A set of disruptions in DN and QDN configurations adapted to DEMO conditions has been simulated by means of MAXFEA code using the recent DEMO 2020 reference geometry [17]. The simulated configurations are a symmetric DN and two QDN, upper and lower (UQDN and LQDN), shown in Figure 40. The symmetric DN DEMO configuration has been developed based on official WPPMI DN @ EOF, whilst the QDN have been modelled moving the secondary null at distance Δ_{DEMO} from the separatrix. The distance has been scaled from JET (Δ_{JET} =0.38 m obtained from the CREATE-NL equilibrium reconstruction at 46.6 for the pulse #68805), and using the following equation (1):

$$\Delta_{DEMO} = \Delta_{JET} \cdot \frac{R_{0-DEMO}}{R_{0-JET}} \qquad (1)$$

where R_0 is the related machine major radius, $R_{0\text{-JET}}$=2.96 m and $R_{0\text{-DEMO}}$=8.95 m. Δ_{DEMO}results in 1.15 m.

Accepted Manuscript

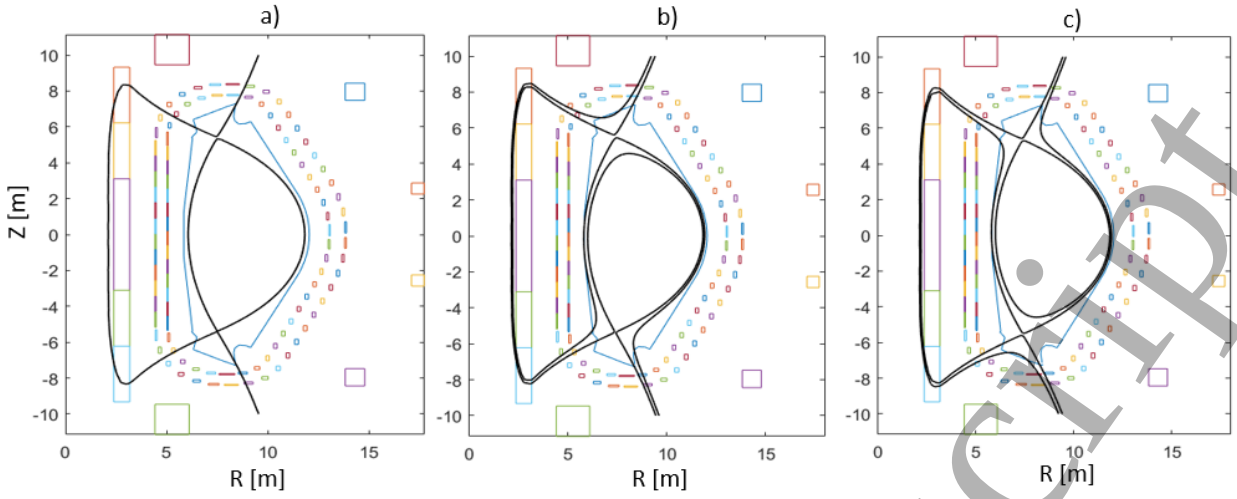

Figure 40. simulated DEMO configurations: a) official WPPMI – DN @ EOF symmetric DN, b) perturbed DN: LQDN ; c) perturbed DN: UQDN. The perturbed ones have been modelled moving the secondary null at a distance from the separatrix of ≈1.15 m (from equation (1)).

For each DEMO configuration shown in Figure 40, a destabilizing drop of β_{pol} occurring 10 ms after the start of simulation is applied to set up the MD, which is followed by the loss of position control (VDE phase). The CQ durations has been set to ~78 ms (Fast MD). The halo and eddy currents and the EM loads on VV have been evaluated for a time window lasting 250 ms. The simulation results are shown in Figures 41–43 for DN, LQDN and UQDN respectively, and summarized in Table 7. For each case: subplot a) reports the plasma separatrix at VDE starting point and the trajectory of the plasma centroid during the VDE phase (solid blue line); subplot b) reports the halo current (red), the eddy currents on the upper VV (blue), the eddy currents on the lower VV (green) and the total eddy currents (yellow); subplot c) reports the electromagnetic vertical forces on VV due to halo current (orange), eddy current (blue) and their sum (yellow). In both subplots b) and c), the purple line is the simulated plasma current.

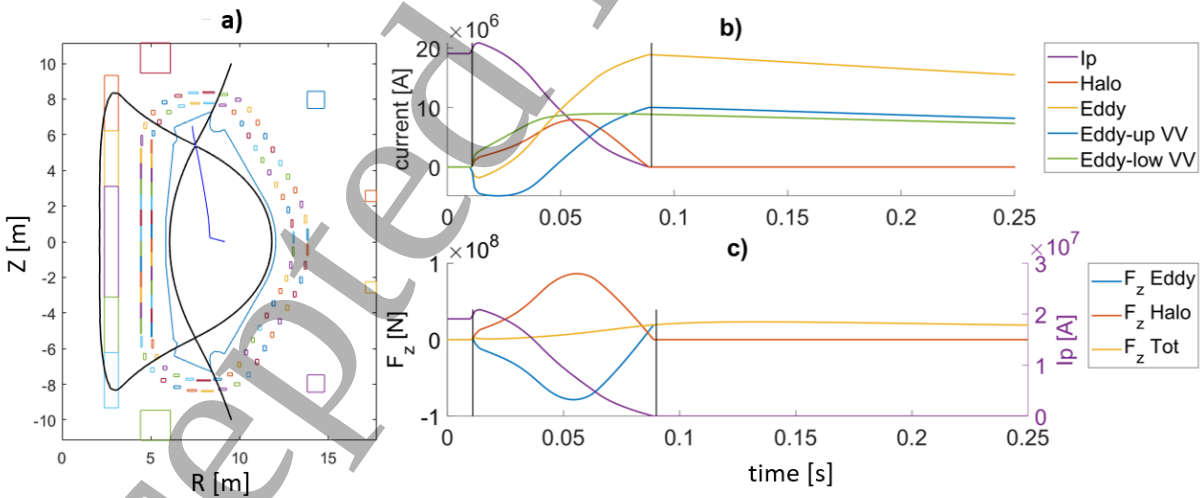

Figure 41. DEMO DN MAXFEA simulation: a) plasma separatrix at VDE phase starting point (black solid line), plasma trajectory during VDE (solid blue line); b) plasma current (purple line), halo current (red line), overall eddy current (yellow line), upper VV eddy currents (blue line) and lower VV eddy currents (green line); c) EM loads on VV: eddy (blue), halo (red) and the total (yellow) vertical forces.

Accepted Manuscript

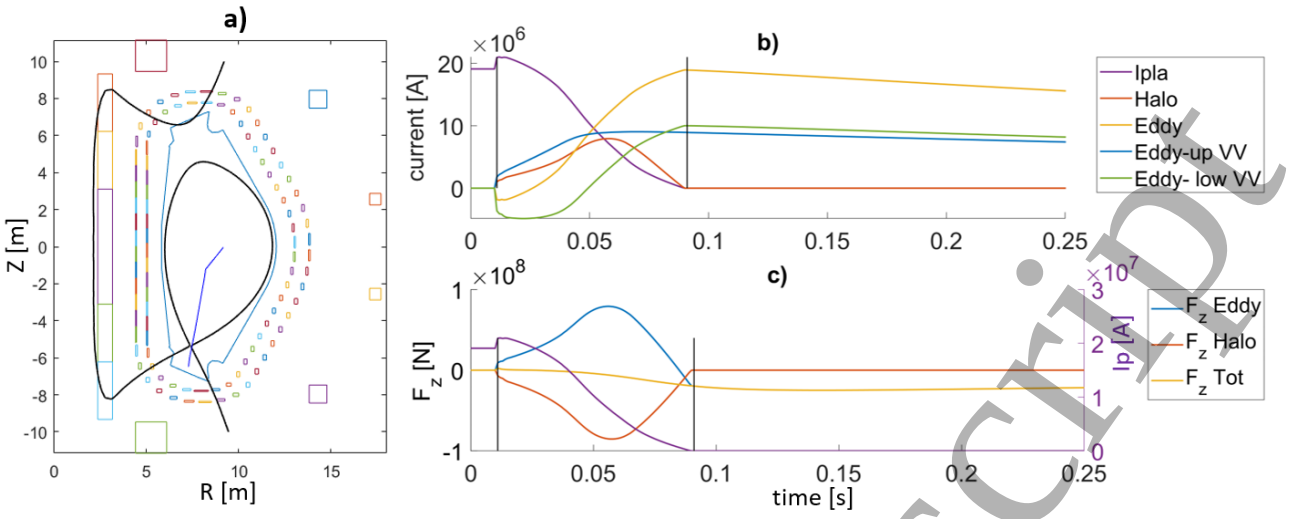

Figure 42. MAXFEA simulation of DEMO perturbed DN (LQDN): a) plasma separatrix at VDE starting point (red solid line), plasma trajectory during VDE (solid blue line); b) plasma current (purple line), halo current (red line), overall eddy current (yellow line), upper VV eddy currents (blue line) and lower VV eddy currents (green line); c) EM loads on VV: simulated eddy (blue) halo (red) and total (yellow line) vertical forces.

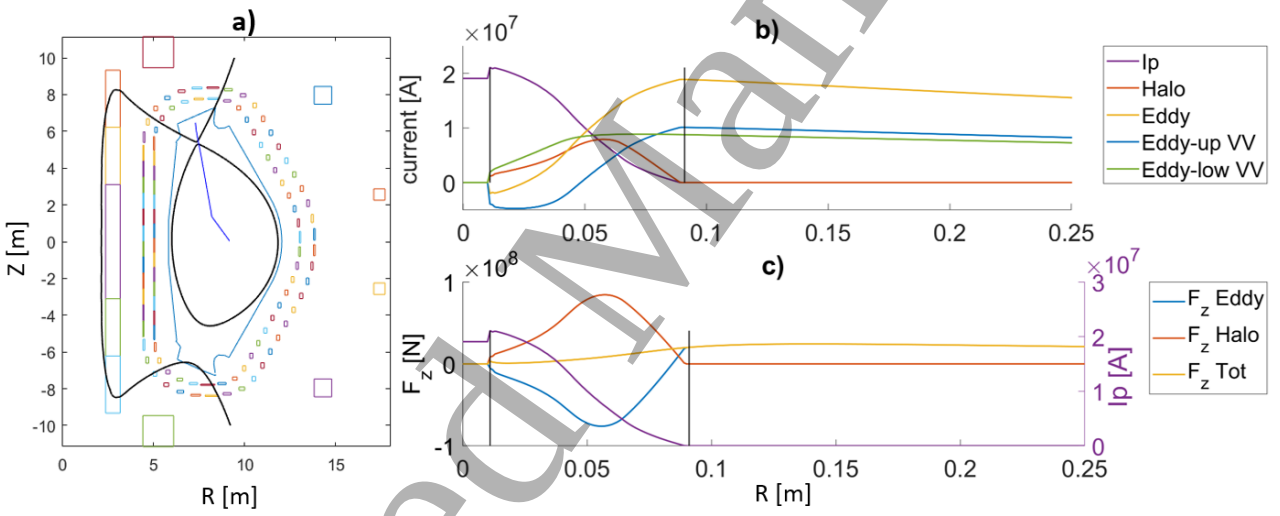

Figure 43. MAXFEA simulation of DEMO perturbed DN (UQDN): a) plasma separatrix at VDE starting point (black solid line), plasma trajectory during VDE (solid blue line); b) plasma current (purple line), halo current (red line), overall eddy current (yellow line), upper VV eddy currents (blue line) and lower VV eddy currents (green line); c) EM loads on VV: Simulated eddy (blue), halo (red) and total (yellow) vertical forces.

Table 7 summarizes the simulation results in terms of $I_{halo\text{-}max}$, maximum axisymmetric index and $F_{z\text{-}max}$. As expected, similar results have been found in terms of total vertical force. Furthermore, the three analysed configurations resulted comparable in terms of halo currents.

Accepted Manuscript

Table 7. JET pulse #68805 scaled to DEMO 2020 reference geometry, in symmetric DN and perturbed UQDN and LQDN.

Configuration	Event	$I_{halo-max}$ [MA]	Axisym-max halo	F_{z-max} [MN]
DN	Fast Type 3 VDE	~ 8	~ 0.4	~ 23.5
LQDN	Fast Type 3 VDE	~ 7.9	~ 0.4	~ -24.9
UQDN	Fast Type 3 VDE	~ 7.9	~ 0.4	~ 24.4

6. Conclusions

In this paper, an intermachine database is presented aiming at collecting transient experimental plasma perturbations (ELMs, L-H/H-L transitions and mDs) and VDEs from JET-ILW, JET-CW and AUG full tungsten wall. Dedicated algorithms have been developed by the authors to collect discharges affected by the considered plasma perturbations and to support the database construction. The database contains information needed to develop the analysis about the implication of the plasma perturbations on the plasma vertical stability from physical and engineering standpoints. The settled database reports the pulse characteristic times and the perturbation occurrence time window. Each perturbation is featured by the values at its own reference times of l_i, β_{pol}, Z_c and R_c, and/or their variations in a prefixed time window. In addition, information about the plasma configuration at the reference times and the power from each additional heating system is provided.

In this paper, the analysis devoted to physical characterization of the vertical stability during ELMs and L-H/H-L transitions during dedicated JET experiments reveals the correlation the plasma centroid vertical displacement w.r.t. the l_i and β_{pol} variations during the perturbations to be in a good agreement with previous experimental observations and discussed with respect previous studies.

Therefore, an extensive study aimed at predictive analyses to foresee the plasma position during the evolution of a VDE has been developed, starting from experimental behaviour, and properly scaled to DEMO. As first step, numerical simulation of experimental H-L and mD perturbations followed by hot VDEs have been performed for JET and AUG machines by means of MAXFEA code. The MAXFEA pulses have been properly scaled to DEMO and used as guideline in the investigation of plasma evolution during VDEs, with different configurations. Moreover, predictive simulation of EM loads during the VDE phase has been performed for JET. The simulations of plasma behaviour and the EM loads show a reasonable agreement between interpretative numerical simulations and the experimental data. Consequently, predictive simulations of the evolution of the plasma centroid trajectory, of halo and eddy currents on VV, and of the corresponding EM loads during the VDE phase for EU-DEMO design. A set of possible MDs and hot VDEs (upper and lower) occurring in SN configuration at the start or the end of the flat-top phase, considering two different CQ durations (slow and fast), have been defined according to ITER Physics classification and then simulated. Considering higher halo current and vertical force on VV, the worst case resulted in the upper VDE occurring at the end of the flat-top phase by considering a slow CQ, with $I_{halo-max} \approx 3.7$ MA and $F_{z-max} \approx 61.7$ MN for DEMO machine. For this case, the limiter contact points during the VDE evolution have been predicted. In DN, a symmetric configuration and two perturbed configurations (UQDN and LQDN) have been extrapolated to DEMO 2020 reference geometry. The LQDN resulted to be the worst configuration, in terms of higher vertical force on VV, with $F_{z-max} \approx 24.9$ MN, in case of VDE following a MD with fast CQ.

Accepted Manuscript

Acknowledgments

This work has been carried out within the framework of the EUROfusion Consortium and received funding from the EURATOM research and training programme 2014–2018 and 2019-2020 under grant agreement No 633053. The views and opinions expressed herein do not necessarily reflect those of the European Commission.

The Authors would like to thank Giovanni Artaserse, Michael Faitsch, Fernanda Rimini, Joerg Hobirk, and Irene Zammuto for their support and the useful discussions. Also, thanks to Marco Wischmeier, Albrecht Herrmann, Markus Teschke, Hartmut Zohm for fruitful comments and suggestions.

References

[1] G. Federici, et al., Overview of the design approach and prioritization of R&D activities towards an EU DEMO, Fusion Eng. Des. 109–111 (2016) 1464–1474

[2] R. Wenninger, et al., The physics and technology basis entering European systemcode studies for DEMO, Nucl. Fusion 57 (2017) 016011

[3] H. Utoh, et al., Studies of the plasma vertical instability and its stabilized concepts in JA and EU broader approach, DEMO design activity, Fusion Eng. Des. 136 (2018) 874–877

[4] F. Cismondi, et al., Progress in EU Breeding Blanket design and integration, Fusion Eng. Des. 136 (2018) 782-792

[5] F. Maviglia, et al., Wall protection strategies for DEMO plasma transients, Fusion Eng. Des. 136 (2018) 410-414

[6] F. Maviglia, et al., Impact of plasma-wall interaction and exhaust on the EU-DEMO design, Nuclear Mat. Energ. 26 (2021) 100897

[7] R. Albanese, et al., Overview of modelling activities for Plasma Control Upgrade in JET, Fusion Eng. Des. 86 (2011) 1030-1033

[8] ITER Physics Basis Expert Groups on Confinement and Transport and Confinement Modelling and Database, ITER Physics Basis Editors 1999 Nucl. Fusion 39 2175

[9] H. Zohm, Magnetohydrodynamic Stability of Tokamaks, 2015 Wiley-VCH Verlag GmbH & Co. KGaA.

[10] D.A. Humphreys, et al., Experimental vertical stability studies for ITER performance and design guidance Nucl. Fusion 49 (2009) 115003

[11] F. Maviglia, et al., Impact of plasma thermal transients on the design of the EU DEMO first wall protection, Fusion Eng. Des. 158 (2020) 111713.

[12] R. Albanese, Electromagnetic analyses of single and double null configurations in DEMO device, Fusion Eng. Des. 146 (2019) 1468-1472.

[13] R. Albanese, R. Ambrosino and M. Mattei, "CREATE-NL+: a robust control-oriented free boundary dynamic plasma equilibrium solver", Fusion Eng. Des. 96 (2015) 664–667

[14] F. Villone, et al., Coupling of nonlinear axisymmetric plasma evolution with three dimensional volumetric conductors, Plasma Phys. Control. Fusion 55 (2013) 095008

[15] F. Maviglia, et al., Optimization of DEMO geometry and disruption location prediction, Fusion Eng. Des. 146 (2019) 967-971

[16] G. Federici, et al., DEMO design activity in Europe: progress and updates, Fusion Eng. Des. 136 (2018) 729–741.

[17] T. Franke, et al, "The EU DEMO equatorial outboard limiter — Design and port integration concept", Fusion Eng. Des. 158 (2020) 111647

[18] P. Barabaschi, The MAXFEA code, Proceedings Plasma Control Technical Meeting, Naka, Japan, April 1993

[19] R. Lombroni, et al., Using MAXFEA code in combination with ANSYS APDL for the simulation of plasma disruption events on EU DEMO, Fusion Eng. Des., 170 (2021), 112697, https://doi.org/10.1016/j.fusengdes.2021.112697.

[20] F. Maviglia, et al., Optimization of DEMO geometry and disruption location prediction, Fus. Eng. Des., 146 (2019), Part A, 967-971, https://doi.org/10.1016/j.fusengdes.2019.01.127

[21] Zhang, Y., et al, Prediction of disruptions on ASDEX upgrade using discriminant analysis, NF, 2011, 51(6), 063039

[22] A. Pau, et al, A tool to support the construction of reliable disruption databases, Fusion Eng. Des. 125 (2017)139-153

[23] H. Zohm, Edge localized modes (ELMs), Plasma Phys. Control. Fusion 38 (1996) 105-128

Accepted Manuscript

[24] S. Saarelma, et al., Integrated modelling of H-mode pedestal and confinement in JET-ILW, Plasma Phys. Control. Fus., 60(1), 014042 (2017)
[25] Maggi CF, et al, L-H power threshold studies in JET with Be/W and C wall. NUCLEAR FUSION, l Nucl. Fusion 54 (2014) 023007
[26] E. Delabie et al., 2014, Overview and Interpretation of L-H Threshold Experiments on JET with the ITER-like Wal, Proc. 25th Int. Conf. on Fusion Energy (St. Petersburg, Russian Ferderation, 2014) (Vienna: IAEA) EX/P5-24, http://www-naweb.iaea.org/napc/physics/FEC/FEC2014/fec_sourcebook_online.pdf
[27] F. Villone, et al., Vertical stability margin studies on TCV: experiments and modelling, 45th EPS Conference on Plasma Phys., Prague, 2 - 6 July 2018, P-5.1054
[28] I. Nunes, et al., Small ELMs in quasi-double null plasmas at JET, 34th EPS Conference on Plasma Phys. Warsaw, 2 - 6 July 2007, ECA Vol.31F, P-5.137
[29] F.G. Rimini et al., 2008, High Beta Regimes at JET: Progress Towards Steady-State Operation, Proc. 22nd Int. Conf. on Fusion Energy (Geneva, Switzerland, 2008) (Vienna: IAEA) EX/1-2, http://www-naweb.iaea.org/napc/physics/FEC/FEC2008/html/index.htm
[30] E. Fable, et al., The role of the source versus the collisionality in predicting a reactor density profile as observed on ASDEX Upgrade discharges, Nucl. Fusion 59 (2019) 076042
[31] R. Albanese, et al., Plasma Current, Shape, and Position Control in ITER, Fusion Technology, 30:2, 167-183, DOI: 10.13182/FST96-A30749, 1996
[32] T. Bellizio, et al., Control of Elongated Plasma in Presence of ELMs in the JET tokamak, IEEE Transactions on Nuclear Science, Vol. 58, No.4, 2011
[33] C. Bachmann, et al., Initial definition of structural load conditions in DEMO, Fusion Eng. Des. 124, November 2017, Pages 633-637
[34] De Vries, P.C., et al., The impact of the ITER-like wall at JET on disruptions, Plasma Phys. Control. Fusion, 54 (12), 124032 (2012)

Accepted Manuscript